Coherent Θ^+ and $\Lambda(1520)$ photoproduction off the deuteron

A. I. Titov,[1,2,*] B. Kämpfer,[1,3] S. Daté,[4] and Y. Ohashi[4]
[1]*Forschungzentrum Rossendorf, D-01314 Dresden, Germany*
[2]*Bogoliubov Laboratory of Theoretical Physics, JINR, Dubna R-141980, Russia*
[3]*Institut für Theoretische Physik, TU Dresden, D-01062 Dresden, Germany*
[4]*Japan Synchrotron Radiation Research Institute, SPring-8,*
1-1-1 Kouto Mikazuki-cho Sayo-gun Hyogo 679-5198, Japan
(Received 23 June 2005; published 26 September 2005; publisher error corrected 19 October 2005)

We analyze coherent $\Theta^+\Lambda(1520)$ photoproduction in the γd interaction near the threshold. We demonstrate that the effect of the coherent production becomes manifest in a comparison of the nK^+ invariant mass distribution when the pK^- system is on the $\Lambda(1520)$ mass. Our model calculations indicate a sizable contribution of resonant and nonresonant background processes in the $\gamma d \to npK^+K^-$ reaction that generally exceeds the contribution of the coherent resonance channel. However, we find that coherent $\Theta^+\Lambda(1520)$ photoproduction is enhanced relative to the background processes in the forward hemisphere of pK^- pair photoproduction. Moreover, the coherence effect does not depend on the Θ^+ photoproduction amplitude and is defined by the probabilities of $\Lambda(1520)$ photoproduction and the $\Theta^+ \to NK$ transition. Therefore, this effect may be used as an independent method for studying the production mechanism and properties of Θ^+ .

DOI: 10.1103/PhysRevC.72.035206 PACS number(s): 14.20.−c, 13.60.Rj, 13.75.Jz, 13.85.Fb

I. INTRODUCTION

The first evidence for the pentaquark hadron Θ^+ discovered by the Laser Electron Photon at SPring-8 (LEPS) Collaboration [1] was subsequently confirmed in other experiments [2]. However, some other experiments failed to find the Θ^+ signal (for a review see Refs. [3,4]). Since then the situation concerning the existence of the pentaquarks has remained controversial. Independent studies of the manifestation of a Θ^+ state in different processes are, therefore, urgently desired.

Θ^+ photoproduction in the reaction $\gamma d \to npK^+K^-$ seems to be very interesting and important [5,6]. First, it allows one to study simultaneously the $\gamma p \to \Lambda(1520)K^+$ and $\gamma n \to \Theta^+K^-$ subreactions characterized by the similarity in the production mechanisms; i.e., both processes are described by the same set of the tree level Feynman diagrams [7–9]. Therefore, one hopes to define the ratio of Θ^+ to $\Lambda(1520)$ photoproduction with minimal uncertainty of the production mechanisms, which is important for understanding the nature of Θ^+. Second, in case of the γd interaction one can qualitatively study a new basic process—coherent $\Theta^+\Lambda(1520)$ photoproduction. This reaction has its own physics interest and will unambiguously shed new light on pentaquark properties and the mechanism of Θ^+ photoproduction.

It is commonly supposed now that the total width of the Θ^+ is as small as $\Gamma_\Theta \sim 1$ MeV [10], much smaller than the total Λ^* decay width, $\Gamma_{\Lambda^*} \simeq 15.6$ MeV [11]. (Throughout this paper, for simplicity, we use the notation $\Lambda^* \equiv \Lambda(1520)$.) This means that the most promising way to study coherent $\Lambda^*\Theta^+$ production is to analyze the invariant nK^+ mass, M_{nK^+}, distribution at fixed invariant mass of the pK^- pair, M_{pK^-}. Enhancement of Θ^+ photoproduction when M_{pK^-} is in the vicinity of the Λ^* mass would indicate the manifestation of coherent $\Lambda^*\Theta^+$ photoproduction. This particular channel will appear in strong competition with the resonant and nonresonant background processes. By "resonant process" we mean, for example, Λ^* photoproduction from the proton inside the deuteron, when the neutron is a spectator, and similarly Θ^+ photoproduction from a neutron, when the deuteron's proton is a spectator. The term "nonresonant " process denotes K^+K^- photoproduction from a nucleon without excitation of Λ^* or Θ^+. It is clear that coherent photoproduction and the background processes must be analyzed together by using the same theoretical approaches. This allows one to define the kinematic conditions under which the coherent channel manifests itself clearly above strong background processes.

Our aim in the present paper is to discuss these important topics. Our model includes the elementary subprocesses of $\gamma N \to \Lambda^* K$ and $\gamma N \to \Theta^+\bar{K}$ reactions. For the latter we use a model based on the effective Lagrangian approach of Ref. [8], which is, generally speaking, similar to the models developed by other authors in Refs. [12–22]. All these approaches predict the approximate equality of the cross sections of the $\gamma n \to \Theta^+K^-$ and $\gamma p \to \Theta^+\bar{K}^0$ reactions. This equality may be changed into a suppression of the $\gamma p \to \Theta^+\bar{K}^0$ transition [7,23]. However, we are going to demonstrate that the amplitude of the coherent $\Lambda^*\Theta^+$ photoproduction, when Λ^* is produced in the forward hemisphere in the γd center of mass system, is defined by the product of the Λ^* photoproduction amplitude in the γN interaction and the amplitude of the $\Theta^+ \to NK$ transition. In other words, the coherence effect of $\Lambda^*\Theta^+$ photoproduction in the forward hemisphere does not depend on the Θ^+ photoproduction amplitude and remains finite even if the cross section of the $\gamma p \to \Theta^+\bar{K}^0$ reaction is vanishing. The coherence effect in the backward hemisphere is sensitive to the Θ^+ photoproduction amplitude, and it is suppressed in parallel with the suppression of the $\gamma p \to \Theta^+\bar{K}^0$ reaction.

*Electronic address: atitov@rcnp.osaka-u.ac.jp

Our paper is organized as follows. In Sec. II, we discuss resonant Θ^+ and Λ^* photoproduction from a nucleon. In Sec. III, we consider the coherent $\gamma d \to \Lambda^*\Theta^+$ reaction. Our model is similar to the approach of Ref. [24], developed for coherent $\Theta^+\Lambda(\Sigma^0)$ photoproduction from a deuteron. In Sec. IV, we discuss the background processes. We start therefore from an analysis of the nonresonant background in elementary $\gamma N \to \Theta^+\bar{K}$ and $\gamma N \to \Lambda^* K$ reactions. Then we apply these subprocesses to an analysis of the background spectator channels. Finally, we estimate the contribution of the coherent semiresonant processes, which differ from coherent photoproduction by the replacement of one hyperon with NK or $N\bar{K}$ pairs. The results of our numerical calculations are presented in Sec. V. The summary is given in Sec. VI. In Appendix A, we show an explicit form of the transition operators for the resonance amplitude.

II. PHOTOPRODUCTION FROM A NUCLEON

A. Θ^+ photoproduction

The main diagrams for the amplitude of the resonance Θ^+ photoproduction in the reaction $\gamma N \to NK\bar{K}$ are shown in Fig. 1. We neglect here the contribution resulting from photons interacting with the final decay vertex [12]. In view of the chosen kinematics, where the invariant mass of the final KN pair is near the resonance position, this is a good approximation, since in the neglected graphs the Θ^+ is far offshell and the graphs of Figs. 1(a)–1(d) dominate the resonance contribution. From a formal point of view gauge invariance is lost without contributions arising from the electromagnetic interaction in the decay vertex. However, following Ref. [25] for the initial photoproduction process, we construct an overall conserved current by an appropriate choice of the contact term of Fig. 1(d).

In this section k, p, q, $\bar{q}$, and p' denote the four-momenta of the incoming photon, the initial nucleon, the outgoing K and $\bar{K}$ mesons, and the recoil nucleon, respectively. The standard Mandelstam variables for virtual Θ^+ photoproduction are defined by $t = (\bar{q} - k)^2$ and $s \equiv W^2 = (p + k)^2$. The $\bar{K}$ meson production angle θ in the center-of-mass system (c.m.s.) is given by $\cos\theta = \mathbf{k} \cdot \bar{\mathbf{q}}/(|\mathbf{k}||\bar{\mathbf{q}}|)$, and the corresponding solid angle is Ω. We consider the integrated Θ^+ decay distribution. The differential cross section $\gamma N \to \Theta^+\bar{K} \to NK\bar{K}$ as a function the $\bar{K}$ meson production angle and NK invariant mass, M_{nK^+}, at the resonance position with $M_{nK^+} = M_\Theta = 1.54\,\text{GeV}$ is related to the cross section of Θ^+ photoproduction in the $\gamma N \to \Theta^+\bar{K}$ reaction as

$$\left.\frac{d\sigma^R_{fi}}{d\Omega dM_{nK^+}}\right|_{M_{nK^+}=M_\Theta} = \frac{1}{\pi\Gamma_\Theta}\frac{d\sigma^{\Theta^+}_{fi}}{d\Omega}, \tag{1}$$

with Γ_Θ denoting the Θ^+ decay width and

$$\frac{d\sigma^{\Theta^+}_{fi}}{d\Omega} = \frac{1}{64\pi^2 s}\frac{p_{\text{out}}}{p_{\text{in}}}\frac{1}{4}\sum_{m_i,m_f,\lambda_\gamma}\left|A^{\Theta^+}_{m_f;m_i,\lambda_\gamma}\right|^2. \tag{2}$$

Here, A^{Θ^+} is the Θ^+ photoproduction amplitude in the $\gamma N \to \Theta^+\bar{K}$ reaction, m_i and m_f are the nucleon and Θ^+ spin projections, respectively, and λ_γ denotes the incoming photon helicity; p_{in} and p_{out} are the relative momenta in the initial and the final states in the c.m.s., respectively. Further below we will concentrate on the calculation of A^{Θ^+}. For simplicity, in this analysis we limit our consideration to the isoscalar, spin-1/2 Θ^+. Generalization for higher spin [9] may be done in a straightforward manner.

The effective Lagrangians that define the Born terms for the diagrams shown in Figs. 1(a)–1(d) are discussed in many papers (for references see Ref. [8]). Note that different phase conventions are often employed. Therefore, for the sake of definiteness, we list here the effective Lagrangians used in the present work:[1]

$$\mathcal{L}_{\gamma KK} = ie(K^-\partial^\mu K^+ - K^+\partial^\mu K^-)A_\mu, \tag{3a}$$

$$\mathcal{L}_{\gamma\Theta\Theta} = -e\,\bar{\Theta}\left(\gamma_\mu - \frac{\kappa_\Theta}{2M_\Theta}\sigma_{\mu\nu}\partial^\nu\right)A^\mu\Theta, \tag{3b}$$

$$\mathcal{L}_{\gamma NN} = -e\,\bar{N}\left(e_N\gamma_\mu - \frac{\kappa_N}{2M_N}\sigma_{\mu\nu}\partial^\nu\right)A^\mu N, \tag{3c}$$

$$\mathcal{L}^{\pm[\text{PV}]}_{\Theta NK} = \mp\frac{g_{\Theta NK}}{M_\Theta \pm M_N}\bar{\Theta}\Gamma^\pm_\mu(\partial^\mu K)N + \text{h.c.}, \tag{3d}$$

$$\mathcal{L}^{[\text{PV}]}_{\gamma\Theta NK} = -i\frac{eg_{\Theta NK}}{M_\Theta \pm M_N}\bar{\Theta}\Gamma^\pm_\mu A^\mu K N + \text{h.c.}, \tag{3e}$$

$$\mathcal{L}^{\pm[\text{PS}]}_{\Theta NK} = -i\,g_{\Theta NK}\bar{\Theta}\Gamma^\pm K N + \text{h.c.}, \tag{3f}$$

$$\mathcal{L}_{\gamma KK^*} = \frac{eg_{\gamma KK^*}}{M_{K^*}}\epsilon^{\alpha\beta\mu\nu}\partial_\alpha A_\beta\partial_\mu\bar{K}^*_\nu K + \text{h.c.}, \tag{3g}$$

$$\mathcal{L}^\pm_{\Theta NK^*} = -g_{\Theta NK^*}\,\bar{\Theta}\,\Gamma^\mp\left(\gamma_\mu - \frac{\kappa^*}{M_\Theta + M_N}\sigma_{\mu\nu}\partial^\nu\right) \times\bar{K}^{*\mu}N + \text{h.c.}, \tag{3h}$$

where A^μ, Θ, K, and N are the photon, Θ^+, kaon, and the nucleon fields, respectively; K^* stands for the vector kaon field; $\Gamma^\pm_\mu \equiv \Gamma^\pm\gamma_\mu$ (with $\Gamma^+ = \gamma_5$ and $\Gamma^- = 1$ for positive and negative parity, respectively), $e_p = 1, e_n = 0$, and κ_N

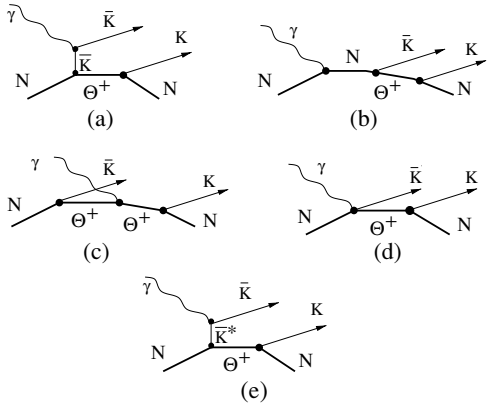

FIG. 1. Tree level diagrams for the reaction $\gamma N \to \Theta^+\bar{K} \to NK\bar{K}$.

[1]Throughout this paper, isospin operators will be suppressed in all Lagrangians and matrix elements for simplicity. They can be easily accounted for in the corresponding coupling constants.

denotes the nucleon anomalous magnetic moment ($\kappa_p = 1.79$ and $\kappa_n = -1.91$), κ_Θ stands for the anomalous magnetic moment of Θ^+, and κ^* denotes the tensor coupling of nucleon and strange vector mesons. The superscripts PS and PV correspond to the pseudo-scalar and pseudo-vector $\Theta^+ NK$ coupling schemes. Equation (3e) describes the contact (Kroll-Ruderman) interaction in the pseudo-vector coupling scheme [see Fig. 1(d)], which does not appear in the case of pseudoscalar coupling [cf. Eq. (3f)].

In calculating the invariant amplitudes, we dress the vertices by form factors. In the present treelevel approach and within our chosen kinematics, only the lines connecting the electromagnetic vertex with the initial $\Theta^+ KN$ vertex correspond to off-shell hadrons. We describe the product of both the electromagnetic and the hadronic form-factor contributions along these off-shell lines by the covariant phenomenological function

$$F(M, p^2) = \frac{\Lambda^4}{\Lambda^4 + (p^2 - M^2)^2}, \tag{4}$$

where p is the corresponding off-shell four-momentum of the virtual particle, M denotes its mass, and Λ stands for the cutoff parameter. The electromagnetic current of the complete amplitude is conserved by making the initial photoproduction process gauge invariant. To this end, we apply the gauge invariance prescription by Haberzettl [25] with the modification by Davidson and Workman [26] to construct a contact term for the initial process $\gamma N \to \Theta^+ \bar{K}$ that is free of kinematical singularities. We emphasize that contributions of the latter type are necessary even for pure pseudo-scalar coupling.

Since the coupling scheme and the Θ^+ parity are unknown, one has to define the corresponding parameters in such a way to get the corresponding cross sections independently of Θ^+ parity and the coupling scheme. We follow Ref. [8], where parameters of the model are fixed by a comparison of the resonant Θ^+ photoproduction cross section and nonresonant background with experiment, and it is shown that one can find such a parameter set that parallels the prediction for PS and PV couplings and for positive and negative Θ^+ parity states as well, at least for the unpolarized and single and double polarization spin observables. Therefore, we can limit the present analysis to the PS coupling and a positive Θ^+ parity.

The resonance amplitudes obtained for the γn and γp reactions read as

$$A^{\Theta^+}_{fi}(\gamma n) = \bar{u}_\Theta(p_\Theta)\big[\mathcal{M}^s{}_\mu + \mathcal{M}^t{}_\mu + \mathcal{M}^u{}_\mu + \mathcal{M}^c{}_\mu + \mathcal{M}^t{}_\mu(K^*)\big] u_n(p)\, \varepsilon^\mu, \tag{5a}$$

$$A^{\Theta^+}_{fi}(\gamma p) = \bar{u}_\Theta(p_\Theta)\big[\mathcal{M}^s{}_\mu + \mathcal{M}^u{}_\mu + \mathcal{M}^c{}_\mu + \mathcal{M}^t{}_\mu(K^*)\big] u_p(p)\, \varepsilon^\mu. \tag{5b}$$

The explicit forms of the transition operators $\mathcal{M}^i_\mu$ for the $\gamma n \to \Theta^+ K^-$ and $\gamma p \to \Theta^+ \bar{K}^0$ reactions are presented in Appendix.

For a positive Θ^+ parity the coupling constant $g_{\Theta NK}$ is found from the Θ^+ decay width as

$$\Gamma_\Theta = \frac{[g_{\Theta NK}]^2 p_F}{2\pi M_\Theta}\Big(\sqrt{M_N^2 + p_F^2} - M_N\Big). \tag{6}$$

We choose a small width, $\Gamma_\Theta = 1$ MeV [10], assuming that the observed width in the invariant mass distribution is determined by the experimental resolution. The magnitude of the coupling constant $g_{\gamma KK^*}$ is extracted from the width of the $K^* \to \gamma K$ decay [11]. Its sign is fixed by SU(3) symmetry. This delivers $e g_{\gamma K^0 K^{*0}} = -0.35$ and $e g_{\gamma K^\pm K^{*\pm}} = 0.23$. The contribution of the s channel [Fig. 1(b)] is small, causing a rather weak dependence of the total amplitude on the tensor coupling κ_Θ in the $\gamma\Theta\Theta$ vertex within a reasonable range of $0 \lesssim |\kappa_\Theta| \lesssim 0.5$ [27]. Therefore, we can choose $\kappa_\Theta = 0$. The coupling constant $g_{\Theta NK^*}$ is written as $g_{\Theta NK^*} = \alpha_\Theta g_{\Theta NK}$, where the parameter α_Θ depends on the choice of the tensor coupling κ^* in Eq. (3h) and cutoff parameters Λ_{K^*} in the form factors of the K^* exchange amplitude. Increasing the value of Λ_{K^*} leads to a decreasing α_Θ. Following Ref. [8], we use $\Lambda_{K^*} = 1.5$ GeV and $\alpha_\Theta = 1.875$ at $\kappa^* = 0$. This value of α_Θ is close to the quark model estimates $\alpha_\Theta = \sqrt{3}$ [28].

Another cutoff parameter, Λ_B, defines the Born terms of the s, u, and t channels and the current-conserving contact terms. Note that the inclusion of the Σ and Λ photoproduction processes [29] results in a larger ambiguity in the choice of Λ_B, which varies from 0.5 to 2 GeV depending on the coupling scheme, the method of conserving the electromagnetic current, etc. Analysis of the vector meson photoproduction [30] and $\gamma n \to \Theta^+ K^-$ favors a small value of the cutoff, $\Lambda_B \simeq 0.5$ GeV. For the $\gamma p \to \Theta^+ \bar{K}^0$ reaction the K^* exchange channel remains dominant at $\Lambda_B \leqslant 1.5$ GeV, and, therefore, in this paper we use a universal value, $\Lambda_B \simeq 0.5$ GeV, for all Born terms.

In Fig. 2 we show the differential cross sections of the reactions $\gamma n \to \Theta^+ K^-$ [Fig. 2(a)] and $\gamma p \to \Theta^+ \bar{K}^0$ [2(b)] in the c.m.s. at $E_\gamma = 2$ GeV. One can see that the t-channel K^* exchange depicted in Fig. 1(e) gives the dominant contribution compared with the Born terms shown in Fig. 1(a)–1(d) in both reactions.

B. $\Lambda(1520)$ photoproduction

The main diagrams for the amplitudes of the excitation of the Λ hyperon in the $\gamma N \to NK\bar{K}$ reaction at low energies are shown in Fig. 3. As for the Θ^+ photoproduction, we neglect the photon interaction within the decay vertex and restore the gauge invariance by a proper choice of the contact terms. The Mandelstam variables for the virtual Λ^* photoproduction are defined by $t = (q - k)^2$, $s \equiv W^2 = (p + k)^2$. The K meson production angle θ (in γp c.m.s.) is given by $\cos\theta = \mathbf{k} \cdot \mathbf{q}/(|\mathbf{k}||\mathbf{q}|)$.

For the description of the Λ^* excitation with $J^P = \frac{3}{2}^-$ we use the following effective Lagrangians [30,31]:

$$\mathcal{L}_{\Lambda^* NK} = \frac{g_{\Lambda^* NK}}{M_{\Lambda^*}}\, \bar{\Lambda}^*_\mu\, \theta^{\mu\nu}(Z)\, (\partial_\nu \bar{K})\, \gamma_5 N + \text{h.c.}, \tag{7a}$$

$$\mathcal{L}_{\gamma\Lambda^* NK} = -i\frac{e g_{\Lambda^* NK}}{M^*_\Lambda}\, \bar{\Lambda}^*_\mu \gamma_5 A^\mu \bar{K} N + \text{h.c.}, \tag{7b}$$

$$\mathcal{L}^\pm_{\Lambda^* NK^*} = i\frac{g_{\Lambda^* NK^*}}{M_{\Lambda^*}}\, \bar{\Lambda}^*_\mu\, \theta^{\mu\nu}(Y) \gamma^\lambda F_{\bar{K}\lambda\nu} N + \text{h.c.}, \tag{7c}$$

where Λ^* is the $\Lambda(1520)$ field, M_{Λ^*} denotes the Λ^* mass, and $F^{\mu\nu}_K$ is related to the vector K^* meson field as

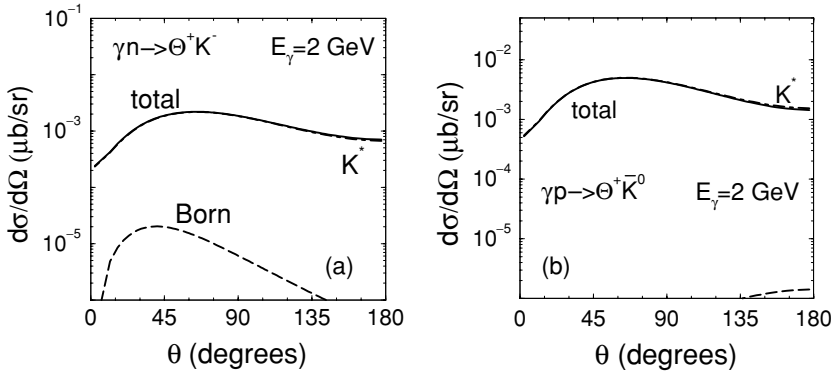

FIG. 2. Differential cross section of the reaction $\gamma n \to \Theta^+ K^-$ (a) and $\gamma p \to \Theta^+ \bar{K}^0$ (b) at $E_\gamma = 2$ GeV. The label "Born" corresponds to the coherent sum of the t, s, u-exchange diagrams and the contact term, shown in Fig. 1(a)–1(d), respectively. Solid curves indicate the total of all contributions. The contribution of K^* exchange is indicated and shown as dashed-dotted curves that almost overlap the solid curves.

$F_K^{\mu\nu} = \partial^\nu K^{*\mu} - \partial^\mu K^{*\nu}$. The operator $\theta_{\mu\nu}(X)$ is a function of the off-shell parameter X: $\theta_{\mu\nu}(X) = g_{\mu\nu} - (\frac{1}{2} + X)\gamma_\mu\gamma_\nu$. In this paper we consider a kinematical region where the invariant mass of the outgoing $N\bar{K}$ pair is close to M_{Λ^*}, Λ^* is almost on-shell, and, therefore, the contribution from terms proportional to $\gamma_\mu\gamma_\nu$ in $\theta_{\mu\nu}(X)$ disappears. This means that $\theta_{\mu\nu}(X)$ may be replaced with $g_{\mu\nu}$. We assume a vanishing value of the anomalous magnetic moment of Λ^* and, therefore, neglect the $\Lambda^*\gamma$ interaction and, correspondingly, the contribution of the u channel shown in Fig. 3(c). All vertices are dressed by the form factors similarly to the case of the Θ^+ photoproduction with the same cutoff parameters. The amplitudes for the $\gamma p \to \Lambda^* K^+$ and $\gamma n \to \Lambda^* K^0$ reactions read as

$$A^{\Lambda^*}{}_{fi}(\gamma p) = \bar{u}^\sigma_{\Lambda^*}(p^*_\Lambda)\big[\mathcal{M}^s{}_{\sigma\mu} + \mathcal{M}^t{}_{\sigma\mu} + \mathcal{M}^c{}_{\sigma\mu} + \mathcal{M}^t{}_{\sigma\mu}(K^*)\big]u_p(p)\,\varepsilon^\mu, \quad (8a)$$

$$A^{\Lambda^*}{}_{fi}(\gamma n) = \bar{u}^\sigma_{\Lambda^*}(p^*_\Lambda)\left[\mathcal{M}^s{}_{\sigma\mu} + \mathcal{M}^t{}_{\sigma\mu}(K^*)\right]u_n(p)\varepsilon^\mu. \quad (8b)$$

The explicit transition operators $\mathcal{M}^i_{\sigma\mu}$ for these reactions are listed in Appendix.

The coupling constant $g_{\Lambda^* NK}$ is found from the Λ^* decay width,

$$\Gamma_{\Lambda^* \to N\bar{K}} = \frac{[g_{\Lambda^* NK}]^2 p_F^3}{6\pi M^3_{\Lambda^*}}\left(\sqrt{M_N^2 + p_F^2} - M_N\right), \quad (9)$$

where p_F is $\Lambda^* \to N\bar{K}$ decay momentum. Taking $\Gamma_{\Lambda^* \to N\bar{K}} \simeq 0.45 \times 15.6$ MeV [11], one finds $|g_{\Lambda^* NK}| = 32.6$.

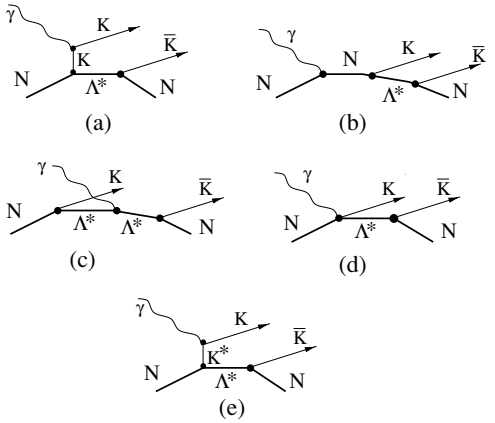

FIG. 3. Tree level diagrams for the reaction $\gamma N \to \Lambda^* K \to N K \bar{K}$.

By analogy to the above considered Θ^+ photoproduction we denote $g_{\Lambda^* NK^*} = \alpha_{\Lambda^*} g_{\Lambda^* NK}$. The parameter α_{Λ^*} must be defined by a comparison of calculated cross sections with experimental data at $E_\gamma \sim 2$ GeV. However, the available experimental data for the $\gamma p \to \Lambda^* K^+$ reaction cover the energy range $E_\gamma = 2.8$–4.8 (GeV) [32], beyond the applicability of the effective Lagrangian formalism. Thus, in this region the total cross section decreases with energy as $E_\gamma^{-2.1}$, whereas the amplitudes of Eq. (8) predict a strong increase. The energy dependence at high energy is reasonably well described by the Regge phenomenology. Since the Λ^* decay angular distribution supports the dominance of the t-channel natural parity exchange processes, one can assume that the dominant contribution to the Λ^* photoproduction at high energy comes from the leading K^* trajectory [33]. The corresponding amplitude is obtained from the t-channel K^* meson exchange in Eq. (8) by the Reggezation of the K^* meson exchange propagator, i.e.,

$$\frac{1}{t - M^2_{K^*}} \to \gamma(t)\left(\frac{s}{s_0}\right)^{\alpha(t)}, \quad (10)$$

where $\alpha(t) = \alpha(0) + \alpha' t$ is the Regge trajectory and $\gamma(t)$ denotes the normalization function

$$\gamma(t) = C_R(\mathrm{Tr}[R\,R^\dagger])^{-1}, \qquad R = \bar{u}^\sigma_{\Lambda^*}(p^*_\Lambda)\left[\varepsilon^{\nu\mu\alpha\beta}\,k^\nu q'^\alpha\left(q'_\sigma\gamma^\beta - \not{q}' g^\beta_\sigma\right)\right]u_n(p)\,\varepsilon^\mu, \quad (11)$$

with $q' = p_{\Lambda^*} - p$. In the following we assume that at energies near the threshold the production amplitude is defined by the effective Lagrangian model of Eq. (8), $A^{\Lambda^*}_{\text{eff. L.}}$, whereas at high energies it is described by the Regge phenomenology, $A^{\Lambda^*}_R$, as

$$A^{\Lambda^*} = A^{\Lambda^*}_{\text{eff. L.}}\,\theta(E_0 - E_\gamma) + A^{\Lambda^*}_R\,\theta(E_\gamma - E_0). \quad (12)$$

We take $E_0 = 2.3$ GeV as the matching point between the two regimes. The choice of parameters in Eqs. (10) and (11) as $s_0 = 1$ GeV, $\alpha(t) = -0.1 + 0.9t$, and $C_R = 29.6$ gives a satisfactory description of the high energy data, as exhibited in Fig. 4 for the differential cross section at $E_\gamma = 3.7$ GeV.

In Fig. 5 we show the energy dependence of the total cross section. The dot-dashed curve is the fit of the data $\sigma \simeq 6.55\,(E_\gamma/\mathrm{GeV})^{-2.1}$ (μb) from Ref. [32]. For illustration we also show the cross section calculated with a constant amplitude, where the energy dependence is defined by the phase space volume alone. The strength parameter α_{Λ^*} is

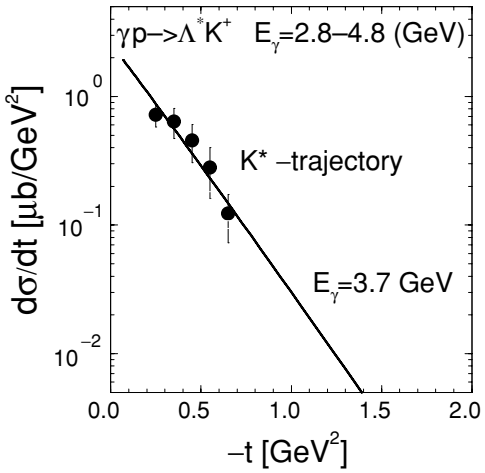

FIG. 4. Differential cross section of the reaction $\gamma p \to \Lambda^+ K^+$ at $E_\gamma = 3.7$ GeV. Experimental data from Ref. [32].

adjusted by fitting the calculated cross section to the experimental extrapolation (dot-dashed curve) at the normalization point. Two solutions $\alpha_{\Lambda^*} = +0.372$ and -0.657 result in two different energy dependencies of the cross section at low energy. Both solutions exceed the experimental data above the normalization point. The solution with positive α_{Λ^*} at low energies is close to the pure phase space dependence shown by the long-dashed curve.

In Fig. 6 we show the differential cross sections of the Λ^* photoproduction at $E_\gamma = 2$ GeV. The differential cross sections of the $\gamma p \to \Lambda^* K^+$ reaction for positive α_{Λ^*} together with the separate contributions of the Born and K^* exchange

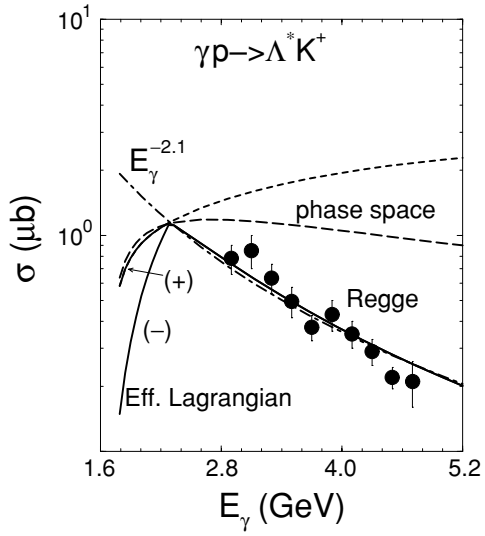

FIG. 5. Total cross section of the reaction $\gamma p \to \Lambda^* K^+$ as a function of the photon energy. The experimental data are taken from Ref. [32]. The dot-dashed curve is the fit of this data $\sigma \simeq 6.55\, E_\gamma^{-2.1}$ (μb). The long-dashed curve represents the cross section when the amplitude is taken to be constant. The solid curves corresponds to the amplitude of Eq. (12). The signs $\pm$ corresponds to the sign of α_{Λ^*}. The dashed curve describes the extrapolation of the effective Lagrangian model to the high energy region.

channels are shown in Fig. 6(a). In case of the $\gamma n \to \Lambda^* K^0$ reaction, shown in Fig. 6(b) by the solid curve, the Born term (s-channel exchange) is negligible. In the γp reaction, the interplay of the Born terms and the K^* exchange amplitude is important at forward angles, which leads to a dependence of the total cross section on the sign of α^*_Λ [see Fig. 6(b)]. However, as we will see below, in the coherent $\gamma d \to \Lambda^* \Theta^+$ reaction the region of backward angles of the K^+ photoproduction gives the main contribution, and, therefore, the final result is not sensitive to the choice of the solution. Nevertheless, for further consideration we chose the solution with positive α_{Λ^*} because it describes the total K^+K^- production better in γp interaction at low energies.

Finally, we note that a similar approach for the Λ^* photoproduction based on the effective Lagrangian formalism was developed in a recent paper [7]. The difference consists in a different choice of the form factors and parameters, which results in slightly different predictions for the differential and total cross sections. This difference may be resolved experimentally.

III. REACTION $\gamma d \to \Lambda^* \Theta^+$

The tree level diagrams for the coherent $\gamma d \to \Lambda^* \Theta^+$ photoproduction are shown in Fig. 7.

First of all note that the amplitudes from the charge and neutral meson exchange shown in Figs. 7(a) and 7(c) and/or 7(b) and 7(d) give constructive interference in the total cross section. That is because in the elementary amplitudes of $\gamma N \to \Lambda^* K$ and $\gamma N \to \Theta^+ \bar{K}$ reactions the dominant contribution comes from the K^* exchange. The different signs in $\gamma K^{0*} \bar{K}^0$ and $\gamma K^{+*} K^-$ vertices are compensated by the different signs in $n\Theta^+ K^-$ and $p\Theta^+ \bar{K}^0$ interactions. The latter is a consequence of the assumed isospin $I = 0$ of the pentaquark.

The amplitudes of the coherent $\Lambda^* \Theta^+$ photoproduction are expressed through the transition operators of the elementary processes $\gamma N \to \Lambda^* K$ and $\gamma N \to \Theta^+ \bar{K}$ shown in Figs. 7(a), 7(c) and 7(b), 7(d), respectively, as

$$A_{(a,c)} = g_{\Theta NK} \int \frac{d^4p}{(2\pi)^4}\, \bar{u}_\Theta \gamma_5 \frac{1}{q^2 - M_K^2}\, \bar{u}^\sigma_{\Lambda^*} \mathcal{M}^{\Lambda^*}_{\sigma\mu} \times \frac{\not{p} + M}{p^2 - M^2} \Gamma_d \frac{\not{p}' + M}{p'^2 - M^2} U_d \epsilon^\mu, \tag{13a}$$

$$A_{(b,d)} = -\frac{g_{\Lambda^* NK}}{M^*_\Lambda} \int \frac{d^4p}{(2\pi)^4}\, \bar{u}_\Theta \mathcal{M}^\Theta_\mu \frac{1}{q^2 - M_K^2}\, \bar{u}^\sigma_{\Lambda^*} q_\sigma \gamma_5 \times \frac{\not{p} + M}{p^2 - M^2} \Gamma_d \frac{\not{p}' + M}{p'^2 - M^2} U_d \epsilon^\mu, \tag{13b}$$

where the transition operators $\mathcal{M}$ are described in the previous section, Γ_d and U_d stand for the deuteron np coupling vertex and the deuteron spinor, respectively, $p' = p_d - p$, and q is the momentum of the exchanged kaon.

Following Ref. [24], we assume that the dominant contribution to the loop integrals comes from their imaginary parts, which may be evaluated by summing all possible cuttings of the loops, as shown in Fig. 8.

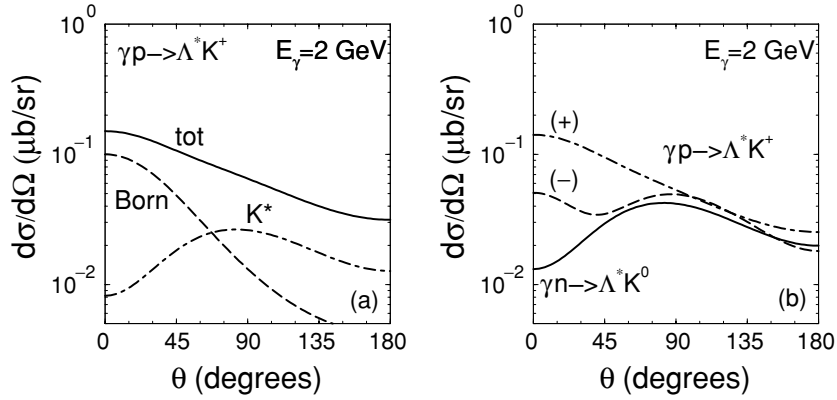

FIG. 6. (a) Differential cross section of the $\gamma p \to \Lambda^* K^+$ reaction at $E_\gamma = 2$ GeV. The notation "Born" corresponds to the coherent sum of the t, s-exchange diagram and the contact term, shown in Figs. 3(a), 3(b), and 3(d), respectively. (b) Differential cross section of the $\gamma n \to \Lambda^* K^0$ reaction (solid curve) and $\gamma p \to \Lambda^* K^+$ reaction (dashed and dot-dashed curves). The symbol $\pm$ indicates the sign of α_{Λ^*}.

Calculating the imaginary parts, we use the following substitutions for the propagators of the on-shell particles (shown by crosses):

$$\frac{1}{q^2 - M_K^2} \to 2\pi\delta\big(q^2 - M_K^2\big),$$
$$\frac{\not{p} + M}{p^2 - M^2} \to 2\pi\,(\not{p} + M)\,\delta(p^2 - M^2), \tag{14}$$

and the identity

$$\int d^4p\delta(p^2 - M^2) = \int \frac{d^3\mathbf{p}}{2E}, \tag{15}$$

with $E^2 = \mathbf{p}^2 + M^2$. We also use the standard representation of the product of the deuteron vertex function and the attached nucleon propagator through the nonrelativistic deuteron function

$$\Gamma_d \frac{\bar{u}_1(p)\bar{u}_2(p_d - p)}{U_d} = \sqrt{2M_d}\,\psi_{m_d,m_1m_2}, \tag{16}$$

where ψ_{m_d,m_1m_2} is the deuteron wave function with the spin projection m_d and the nucleon spin projections m_1 and m_2. By using Eqs. (14)–(16), one can express the principal parts of the invariant amplitudes in Eq. (13) as

$$A^P_{(a,c)} = g_{\Theta NK} \sum_{m_1m_2} [\bar{u}_\Theta(p_\Theta)\gamma_5 u_{m_1}(r)] \times \big[\bar{u}^\sigma_{\Lambda^*}(p^*_\Lambda)\mathcal{M}^{\Lambda^*}_{\sigma\mu}\,\epsilon^\mu u_{m_2}(r)\big]\, S^{\Lambda^*}_{m_1m_2}, \tag{17a}$$

$$A^P_{(b,d)} = -\frac{g_{\Lambda^*NK}}{M^*_\Lambda} \sum_{m_1m_2} [\bar{u}_\Theta \mathcal{M}^\Theta_\mu\, u_{m_1}(r)\epsilon^\mu] \times \big[\bar{u}^\sigma_{\Lambda^*} q_\sigma \gamma_5\, u_{m_2}(r)\big] S^{\Theta^+}_{m_1m_2}, \tag{17b}$$

where $r = p_d/2$ and

$$\begin{aligned} S^{\Lambda^*}_{m_1m_2} &= I^i_{m_1m_2}(p_\Theta) + I^j_{m_1m_2}(k - p^*_\Lambda), \\ S^{\Theta^+}_{m_1m_2} &= I^i_{m_1m_2}(p^*_\Lambda) + I^j_{m_1m_2}(k - p_\Theta), \\ I^{i,j}_{m_1m_2}(p_X) &= i\frac{\sqrt{2M_d}}{16\pi}\int \frac{pdp}{Ep_X}\,\theta(1 - |a_{i,j}(p, p_X)|) \times \phi_{m_d,m_1m_2}(p, a(p, p_X)), \\ a_i(p, p_X) &= \frac{2EE_X + M_K^2 - M_X^2 - M^2}{2pp_X}, \\ a_j(p, p_X) &= \frac{2EE_X - M_K^2 + M_X^2 + M^2}{2pp_X}, \\ \phi_{m_d,m_1m_2}(p, a) &= \sqrt{4\pi}\left\langle \frac{1}{2}m_1\frac{1}{2}m_2 \middle| 1m_d \right\rangle \Big[u_0(p) + \frac{1}{\sqrt{8}}(3a^2 - 1)(1 - 3\,\delta_{m_d0})\,u_2(p)\Big], \end{aligned} \tag{18}$$

where $M_X^2 = E_X^2 - p_X^2$ and u_l with $l = 0, 2$ is the radial deuteron wave function in the momentum space, normalized

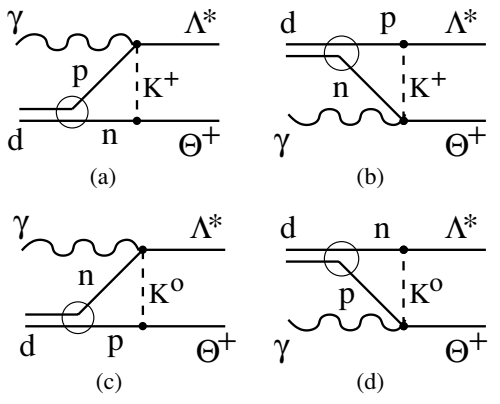

FIG. 7. Tree level diagrams for the reaction $\gamma d \to \Lambda^*\Theta^+$. The exchange of charged and neutral mesons are shown in (a), (b) and in (c), (d), respectively.

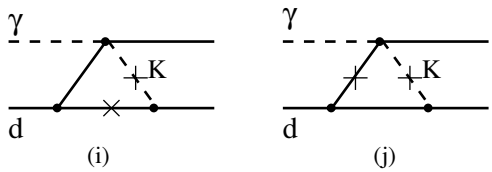

FIG. 8. Diagrammatic representation of cutting (indicated by crosses) in the loop diagrams.

as

$$\int \frac{d^3\mathbf{p}}{(2\pi)^3}\,\Phi(p) = 1,$$

where

$$\Phi(p) = 4\pi\left[u_0^2(p) + u_2^2(p)\right]. \tag{19}$$

In deriving Eqs. (17) we neglect the p dependence of the elementary amplitudes of $\gamma N \to \Lambda^* K$ and $\gamma N \to \Theta^+ \bar{K}$ on p (see Figs. 2 and 4) in comparison with the sharp p dependence of $\Phi(p)$. In our calculation we use the deuteron wave function for the realistic Paris potential [34]. We checked that the final result does not depend on the fine structure of the deuteron wave function and practically does not depend on the choice of the potential.

The differential cross section of the coherent $\Lambda^*\Theta^+$ photoproduction reads as

$$\frac{d\sigma^{\gamma d\to\Lambda^*\Theta^+}}{d\Omega} = \frac{1}{64\pi^2}\frac{1}{S}\frac{P_{\rm out}}{P_{\rm in}}|A_{a,c} + A_{b,d}|^2, \tag{20}$$

where S, $P_{\rm in}$, and $P_{\rm out}$ are the square of the total energy and the momenta in the initial and the final states in γd c.m.s., respectively; averaging and summing over the spin projections in the initial and the final states are assumed. Note that the interference between amplitudes $A_{a,c}$ and $A_{b,d}$ is negligible, and they can be summed incoherently.

In Fig. 9 we show the differential cross section of the reaction $\gamma d \to \Lambda^*\Theta^+$ at $E_\gamma = 2$ GeV as a function of the angle between the beam direction and direction of flight of Λ^* in the γd c.m.s. The nonmonotonous behavior of the cross section is completely defined by the spectral functions S^{Λ^*} and S^{Θ^+} in Eqs. (17a) and (17b), respectively. S^{Λ^*} and S^{Θ^+} have sharp peaks in forward ($\theta_{\gamma\Lambda^*} \simeq 27.5^\circ$) and backward ($\theta_{\gamma\Lambda^*} \simeq 152.5^\circ$) hemispheres, respectively.

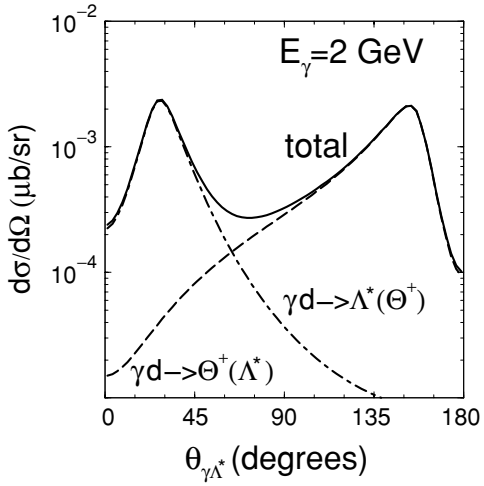

FIG. 9. Differential cross section of the $\gamma d \to \Lambda^*\Theta^+$ reaction. The notation $\gamma d \to \Lambda^*(\Theta^+)$ and $\gamma d \to \Theta^+(\Lambda^*)$ corresponds to the diagrams in Fig. 7(a), 7(c) and in 7(b), 7(d), respectively.

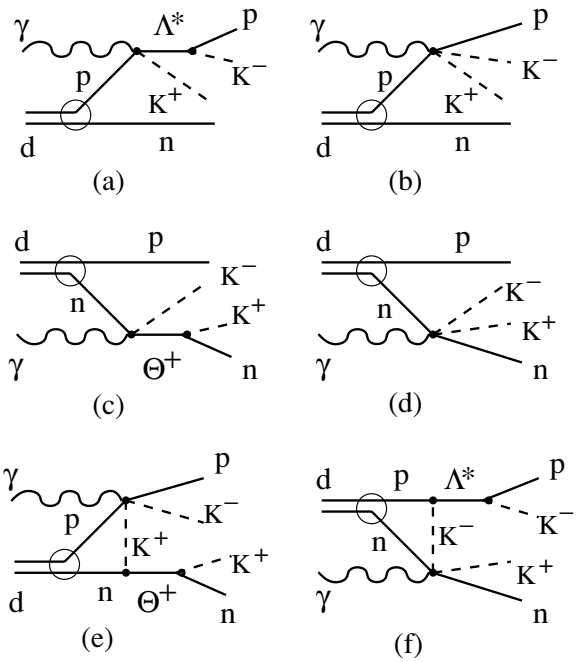

FIG. 10. Tree level diagrams for background processes. (a)–(d) noncoherent spectator channels; (e), (f) coherent semiresonant background processes.

IV. BACKGROUND CONTRIBUTION

Since the Λ^* and Θ^+ are unstable baryons, the typical experiment for studying the coherent $\gamma d \to \Lambda^*\Theta^+$ process must include a simultaneous measurement of the pK^- and nK^+ invariant masses. Therefore, the question is whether the predicted cross section of the coherent $\Lambda^*\Theta^+$ photoproduction is large enough to be seen above the background of competing resonant and nonresonant processes in the $\gamma d \to npK^+K^-$ reaction.

We consider three types of background process. One is the photoproduction of a K^+K^- pair in a γp interaction when the neutron is a spectator. This process includes the resonant $\gamma p \to \Lambda^* K^+ \to pK^+K^-$ photoproduction and the nonresonant $\gamma p \to pK^+K^-$ reaction shown in Figs. 10(a) and 10(b), respectively.

Similarly, a K^+K^- pair can be produced in a γn interaction when the proton is a spectator. The corresponding processes are depicted in Figs. 10(c) and 10(d).

The third process is the coherent background when the K^+K^- pair is produced in a γN interaction and one of the kaons together with the second nucleon forms the outgoing Θ^+ or Λ^*, as shown in Figs. 10(e) and 10(f), respectively. We term it a coherent semiresonant background.

A. Spectator channels

First, let us consider the K^+K^- photoproduction in a γd interaction where the neutron or proton is merely a spectator. As an input, we have to describe the elementary processes $\gamma p \to pK^+K^-$ and $\gamma n \to nK^+K^-$, which consist of resonant and nonresonant parts.

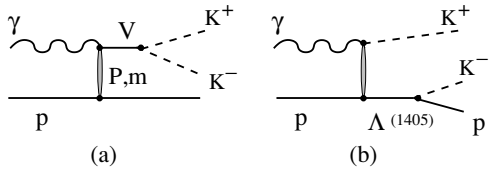

FIG. 11. Background processes for the $\gamma p \to pK^+K^-$ reaction: (a) vector meson contribution; (b) virtual $\Lambda(1405)$ excitation.

1. $\gamma p \to pK^+K^-$

The dominant contribution to the nonresonant part in γp reactions comes from the virtual vector meson decay and $\Lambda(1405)$ excitation [8,22] as depicted in Figs. 11(a) and 11(b). The contribution from excitations of other hyperons is strongly suppressed, since they are far off-shell.

The vector meson channel $\gamma p \to Vp \to pK^+K^-$, where $V = \phi, \rho, \omega$ has been analyzed in detail in Ref. [8]. In the present study we use this model in which the vector mesons are produced through the Pomeron and meson (π, η, σ) exchanges with the same parameters. The only difference from Ref. [8] is that now we do not use a cut on the invariant mass of the K^+K^- pair around the ϕ meson mass.

We parameterize the amplitude of the virtual $\Lambda(1405)$ excitation through the K^* exchange process. This assumption is supported by the K^* exchange dominance in Λ^* and Θ^+ photoproduction and allows us to reduce the number of unknown parameters. The amplitude of this channel reads as

$$\begin{aligned} A_{fi}^{\Lambda'} &= \bar{u}(p')\mathcal{M}_\mu^{\Lambda'} u(p)\varepsilon^\mu, \\ \mathcal{M}_\mu^{\Lambda'} &= -i\frac{eg_{\gamma KK^*}g'}{M_{K^*}\left(t - M_{K^*}^2\right)}\varepsilon^{\mu\nu\alpha\beta}k_\nu q_\alpha \\ &\quad \times \frac{(\not{p}_{\Lambda'} + M_{\Lambda'})\gamma_5\gamma_\beta}{p_{\Lambda'}^2 - M_{\Lambda'}^2 + i\Gamma_{\Lambda'}M_{\Lambda'}} F_{K^*}(t), \end{aligned} \tag{21}$$

where $\Lambda' \equiv \Lambda(1405)$, $\Gamma_{\Lambda'} = 50$ MeV is the total decay width of Λ' [11], $F_{K^*}(t)$ is the K^* exchange form factor, and the constant g' is a product of the two coupling constants $g_{\Lambda' NK}$ and $g_{\Lambda' NK^*}$. The choice $g' \simeq 7.8$ gives the correct value of the total yield of K^+K^- mesons at $E_\gamma \sim 2$ GeV. Note that the interference between the resonance and nonresonance channels in the total cross section is rather weak, and, therefore, they can be added incoherently. Thus, the total cross section of the $\gamma p \to pK^+K^-$ reaction reads as

$$\begin{aligned} \frac{d\sigma}{d\Omega dM_{pK^-}} &= \left(\frac{d\sigma}{d\Omega}\right)^{\gamma p\to\Lambda^*K^+} F^{\Lambda^*}(M_{pK^-}) \\ &\quad + \frac{1}{64\pi^2}\frac{1}{s}\frac{p_{\text{out}}}{p_{\text{in}}}\frac{\bar{q}_F}{16\pi^3} \\ &\quad \times \int \left(\left|A_{fi}^V(\gamma p)\right|^2 + \left|A_{fi}^{\Lambda'}\right|^2\right) d\Omega_F, \end{aligned} \tag{22}$$

where Ω is the solid angle of the K^- meson photoproduction in the γp c.m.s., $\bar{q}_F$ is the momentum of the K^- meson in the c.m.s. of the pK^--pair, and Ω_F is the K^- meson solid angle in this system. Summing and averaging over the spin projection in the initial and the final states is to be included. $F^{\Lambda^*}(M_{pK^-})$ stands for the Λ^* decay distribution, which is obtained straightforwardly from the general expression for the $\gamma p \to pK^+K^-$ amplitude with the virtual excitation of a Λ^* hyperon,

$$F^{\Lambda^*}(M_x) = \frac{\Gamma_{\Lambda^*\to pK^-}}{\pi\Gamma_{\text{tot}}}\frac{2M_xM_{\Lambda^*}\Gamma_{\text{tot}}}{\left(M_x^2 - M_{\Lambda^*}^2\right)^2 + (\Gamma_{\text{tot}}M_{\Lambda^*})^2}, \tag{23}$$

where $\Gamma_{\text{tot}} = 15.6$ MeV and $\Gamma_{\Lambda^*\to pK^-} = (0.45/2) \times \Gamma_{\text{tot}}$ [11].

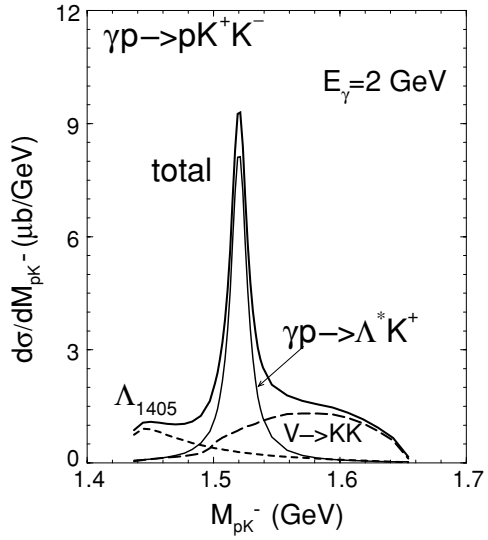

FIG. 12. The pK^- invariant mass distribution in the $\gamma p \to pK^+K^-$ reaction at $E_\gamma = 2$ GeV. The resonance channel, vector meson, and $\Lambda(1405)$ contributions are shown by the inner solid, long dashed, and dashed curves, respectively.

The pK^- invariant mass distribution at $E_\gamma = 2$ GeV integrated over Ω is shown in Fig. 12. One can see that the $\Lambda(1405)$ excitation contributes at M_{pK^-} below the Λ^* resonance position, and the vector meson channels contribute mainly at large M_{pK^-}, above M_{Λ^*}. The partial contributions to the total $\gamma p \to pK^+K^-$ cross section are the following: $\sigma(\Lambda^*) \simeq 0.19\,\mu$b, $\sigma(V) \simeq 0.17\,\mu$b, and $\sigma(\Lambda(1405)) \simeq 0.07\,\mu$b. The total cross section $\sigma_{\text{tot}} \simeq 0.43\mu$b is in agreement with the experimental data of Ref. [35]: $\sigma_{\text{tot}}^{\text{exp}} = (0.47 \pm 0.12)\,\mu$b at $E_\gamma = 2$–2.5 (GeV).

2. $\gamma n \to nK^+K^-$

In this case the nonresonant part is dominated by the vector meson excitation and, therefore, the nK^+ invariant mass distribution may be written in obvious notation as

$$\begin{aligned} \frac{d\sigma}{d\Omega dM_{nK^+}} &= \left(\frac{d\sigma}{d\Omega}\right)^{\gamma n\to\Theta^+K^-} F^{\Theta^+}(M_{nK^+}) \\ &\quad + \frac{1}{64\pi^2}\frac{1}{s}\frac{p_{\text{out}}}{p_{\text{in}}}\frac{q_F}{16\pi^3}\int \left|A_{fi}^V(\gamma n)\right|^2 d\Omega_F, \end{aligned} \tag{24}$$

with

$$F^\Theta(M_x) = \frac{1}{2\pi}\frac{2M_xM_\Theta\Gamma_\Theta}{\left(M_x^2 - M_\Theta^2\right)^2 + (\Gamma_{\text{tot}}M_\Theta)^2}. \tag{25}$$

We will also use the Gaussian distribution taking into account the small Θ^+ decay width and the finite experimental

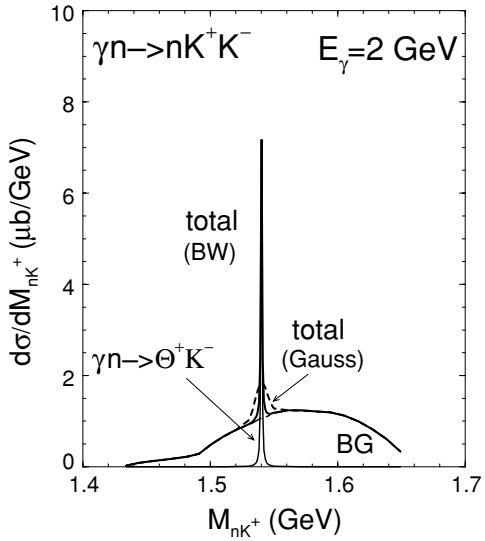

FIG. 13. The nK^+ invariant mass distribution in the $\gamma n \to nK^+K^-$ reaction at $E_\gamma = 2$ GeV. BW indicates the Breit-Wigner Θ^+ decay distribution of Eq. (25). The dashed curve corresponds to a Gaussian distribution of the Θ^+ decay width $\sigma = 5$ MeV.

resolution,

$$F_G^{\Theta}(M_x) = \frac{1}{2}\frac{1}{\sigma\sqrt{2\pi}} e^{-\frac{(M_x - M_\Theta)^2}{2\sigma^2}}. \tag{26}$$

The nK^+ invariant mass distribution at $E_\gamma = 2\,\text{GeV}$ integrated over Ω is shown in Fig. 13. One can see the sharp peak of Θ^+ excitation. In case of a Gaussian Θ^+ decay distribution the peak is modified. The height of the peak is reduced by the factor σ/Γ_Θ, and the width becomes proportional to σ.

3. *Spectator reactions $\gamma d \to pK^+K^-(n)$ and $\gamma d \to nK^+K^-(p)$*

The differential cross section of the $\gamma d \to pK^+K^-(n)$ reaction, where the neutron is a spectator, reads as

$$\begin{aligned}\frac{d\sigma^{\text{sp.(n)}}}{d\Omega dM_{pK^-} dM_{nK^+}} &= \left(\frac{d\sigma}{d\Omega dM_{pK^-}}\right)^{\gamma p \to pK^+K^-} \\ &\quad \times W_{nK}(M_{nK^+}), \\ W_{nK}(M_{nK^+}) &= 2M_{nK^+} \int \frac{d^3\mathbf{p}_n}{(2\pi)^3\sqrt{1 + \mathbf{p}_n^2/M_N^2}} \\ &\quad \times \delta\left(M_{nK^+}^2 - (p_n + q)^2\right)\, \Phi(\mathbf{p}_n),\end{aligned} \tag{27}$$

where we neglect the smooth dependence of $d\sigma^{\gamma p \to pK^+K^-}$ on $\mathbf{p}_n$ in comparison to the sharp $\mathbf{p}_n$ dependence of the momentum distribution in the deuteron, $\Phi(\mathbf{p}_n)$, defined in Eq. (19).

If the invariant mass of the nK^+ pair is not fixed, then the integration over M_{nK^+} leads to the obvious result

$$\int dM_{nK^+} \frac{d\sigma^{\text{sp.(n)}}}{d\Omega dM_{pK^-} dM_{nK^+}} \simeq \left(\frac{d\sigma}{d\Omega dM_{pK^-}}\right)^{\gamma p \to pK^+K^-}. \tag{28}$$

When the invariant mass is fixed, then the function $W_{nK}(M_{nK^+})$ becomes important, and, moreover, it defines mainly the dependence of the cross section on M_{nK^+}. Indeed, let us assume that the momentum distribution in a deuteron behaves as a delta function, i.e., $\Phi(\mathbf{p}) \simeq (2\pi)^3\,\delta(\mathbf{p})$. Then one gets

$$W_{nK}(M_{nK^+}) \simeq 2M_{nK^+}\,\delta\left[M_{nK^+}^2 - \left(M_N^2 + M_K^2 + 2E_{K^+}M_N\right)\right]. \tag{29}$$

That is, the distribution $W_{nK}(M_{nK^+})$ has a peak around the point $M_{nK^+0} \simeq \sqrt{M_N^2 + M_K^2 + 2E_{K^+}M_N}$, which is determined by the energy of the K^+ meson in the laboratory system. On the other hand, this energy depends on the invariant mass of the pK^- pair and the angle of the K^+ production in the γp c.m.s. In reality, the distribution function reads as

$$\begin{aligned}&W_{nK}(M_{nK^+}) \\ &\quad = 2M_{nK^+} \int \frac{pdp}{8\pi^2 q_L \sqrt{1 + p^2/M_N^2}} \Phi(p)\theta(1 - |a|), \\ &a = \frac{2\sqrt{\left(q_L^2 + M_K^2\right)\left(p^2 + M_N^2\right)} + M_N^2 + M_K^2 - M_{nK^+}^2}{2pq_L},\end{aligned} \tag{30}$$

where q_L is the momentum of K^+ meson in laboratory system. The distribution function W_{nK} is shown in Fig. 14(a) as a function of M_{nK^+} at fixed angle of pK^- pair photoproduction, $\theta_{\gamma(pK^-)}$ (in γd c.m.s.) for three different invariant masses of the pK^- pair: $M_{pK^-} = 1.52$, 1.57 and 1.47 GeV. The choice of $\theta_{\gamma(pK^-)} = 27.5^\circ$ corresponds to the position of the maximum of the coherent $\gamma d \to \Lambda^*\Theta^+$ photoproduction cross section at forward angles (see Fig. 9). This angle corresponds to the backward K^+ photoproduction in $\gamma p \to \Lambda^* K^+$: $\theta_{\gamma K^+} \simeq 119^\circ$ in the γp c.m.s.

The differential cross section of the $\gamma d \to nK^+K^-(p)$ reaction, where the proton is spectator, may be obtained from Eq. (27) by using the substitutions $n \to p$, $K^+ \to K^-$, and $M_{nK^+} \to M_{pK^-}$:

$$\frac{d\sigma^{\text{sp.(p)}}}{d\Omega dM_{pK^-} dM_{nK^+}} = \left(\frac{d\sigma}{d\Omega dM_{nK^+}}\right)^{\gamma n \to nK^+K^-} W_{pK}(M_{pK^-}). \tag{31}$$

The essential difference is that now we analyze the dependence of the distribution function W_{pK} not on M_{pK^-} but on the invariant mass M_{nK^+}. This dependence is included in W_{pK} implicitly through the dependence of the momentum of K^- on M_{nK^+}, and therefore, in general, we have no narrow peak structure of W_{pK} as a function of M_{nK^+}. As an example, in Fig. 14(b) we show the distribution W_{pK} as a function of M_{nK^+} at fixed values of $M_{pK^-} = 1.52$, 1.57, and 1.47 GeV and $\theta_{\gamma(pK^-)} = 152.5^\circ$. One can see a broad maximum at $M_{pK^-} = 1.52$ GeV and an almost monotonic behavior at 1.47 and 1.57 GeV.

B. Coherent semi-resonant background

The amplitude of the process shown in Fig. 10(e) is calculated similarly to the amplitude of the coherent $\Lambda^*\Theta^+$

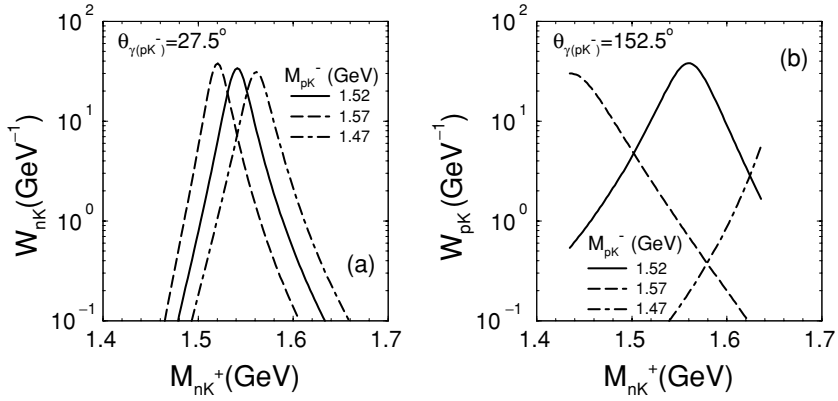

FIG. 14. (a) Invariant mass distribution function W_{nK} as a function of M_{nK^+} at $\theta_{\gamma(pK^-)} = 27.5^\circ$ and fixed values of M_{pK^-}. (b) Invariant mass distribution function W_{pK} as a function of M_{nK^+} at $\theta_{\gamma(pK^-)} = 152.5^\circ$ and fixed values of M_{pK^-}.

photoproduction described by Eq. (17a). The corresponding cross section reads as

$$\frac{d\sigma^e}{d\Omega dM_{pK^-} dM_{nK^+}} = \frac{1}{64\pi^2}\frac{1}{s}\frac{p_{\rm out}}{p_{\rm in}}\frac{\bar{q}_F}{16\pi^3}\frac{1}{2}\left|\frac{d\Omega'}{d\Omega}\right|\int d\Omega_F\,|A_e|^2\,F^{\Theta}(M_{nK^+}), \tag{32}$$

$$A_e = g_{\Theta NK}\sum_{m_1 m_2}[\bar{u}_\Theta(p_\Theta)\gamma_5 u_{m_1}(r)] \times \left[\bar{u}^\sigma_{\Lambda^*}(p^*_\Lambda)\mathcal{M}^{\gamma p\to pK^+K^-}_{\sigma\mu}\varepsilon^\mu u_{m_2}(r)\right]S^{\Lambda^*}_{m_1 m_2},$$

where $p_{\rm in}$, $p_{\rm out}$ are the momenta of the proton and pK^- pair in γp c.m.s., Ω and Ω' are the solid angles of the pK^- pair in γd and γp reactions, respectively, $\bar{q}_F$ is the momentum of the K^- meson in the rest frame of the pK^- pair, and Ω_F is the solid angle of K^- in this frame. The additional factor $1/2$ assumes renormalization of the flux in the γd system compared with the γp interaction. The function $F^\Theta(M_{nK^+})$ is defined in Eq. (25). Averaging and summing over the spin projections in initial and the final states, respectively, have to be performed. Actually, here we have a sum of two cross sections. One is the contribution of the virtual vector meson and another one is the contribution of the virtual $\Lambda(1405)$ excitation.

Similarly, one can write the cross section of the process shown in Fig. 10(f) as

$$\frac{d\sigma^f}{d\Omega dM_{pK^-} dM_{nK^+}} = \frac{1}{64\pi^2}\frac{1}{s}\frac{p_{\rm out}}{p_{\rm in}}\frac{q_F}{16\pi^3}\frac{1}{2}\left|\frac{d\Omega'}{d\Omega}\right|\int d\Omega_F|A_f|^2\,F^{\Lambda^*}(M_{pK^-}), \tag{33}$$

$$A_f = -\frac{g_{\Lambda^* NK}}{M^*_\Lambda}\sum_{m_1 m_2}\left[\bar{u}_\Theta\mathcal{M}^{\gamma n\to nK^+K^-}_\mu u_{m_1}(r)\varepsilon^\mu\right] \times \left[\bar{u}^\sigma_{\Lambda^*}q_\sigma\gamma_5 u_{m_2}(r)\right]S^{\Theta^+}_{m_1 m_2},$$

where the function $F^{\Lambda^*}(M_{pK^-})$ is defined in Eq. (23) and other notation is similar to the previous case.

Let us now compare the contribution of the coherent $\Lambda^*\Theta^+$ photoproduction and the coherent semiresonant background described by Eqs. (33) and (34) in the vicinity of the Θ^+ and Λ^* resonance position:

$$\frac{d\widetilde{\sigma}^{\rm ch.}}{d\Omega} = \int\limits_{M_{\Lambda^*}-\Delta}^{M_{\Lambda^*}+\Delta}\int\limits_{M_\Theta-\Delta}^{M_\Theta+\Delta} dM_{pK^-}\,dM_{nK^+} \times \frac{d\sigma^{\gamma d\to\Lambda^*\Theta^+}}{d\Omega}\,F_{\Lambda^*}(M_{pK^-})\,F_{\Theta^+}(M_{nK^+}),$$

$$\frac{d\widetilde{\sigma}^{\rm ch.bg.}}{d\Omega} = \int\limits_{M_{\Lambda^*}-\Delta}^{M_{\Lambda^*}+\Delta}\int\limits_{M_\Theta-\Delta}^{M_\Theta+\Delta} dM_{pK^-}\,dM_{nK^+} \times \left(\frac{d\sigma^e}{d\Omega dM_{pK^-}dM_{nK^+}} + \frac{d\sigma^f}{d\Omega dM_{pK^-}dM_{nK^+}}\right), \tag{34}$$

where $\Delta = 20$ MeV. In Fig. 15 we show result of such a comparison. One can see that the coherent background contribution has local maxima caused by the spectral functions S, but the values of these contributions at the peak positions are much smaller than for the coherent process. Therefore, the dominant background contribution comes from the spectator processes.

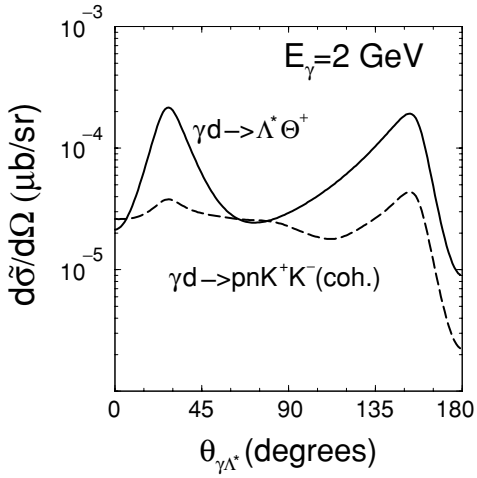

FIG. 15. Comparison of the coherent $\Lambda^*\Theta^+$ photoproduction (solid curve) and coherent semi-resonant background (dashed curve) depicted in Fig. 10(e) and 10(f).

V. RESULTS AND DISCUSSION

As pointed out above, the coherent $\Lambda^*\Theta^+$ photoproduction seems to be accessible most effectively by a search for a sharp Θ^+ peak in the invariant nK^+ mass distribution at fixed invariant masses of the pK^- pair

$$\frac{d\sigma^{\gamma d\to npK^+K^-}(M_0)}{d\Omega dM_{nK^+}} = \int\limits_{M_0-\Delta}^{M_0+\Delta} dM_{pK^-} \frac{d\sigma^{\gamma d\to npK^+K^-}}{d\Omega dM_{nK^+} dM_{pK^-}}. \quad (35)$$

In our further analysis we choose $M_0 = 1.52$, 1.57, and 1.47 GeV and $\Delta = 20$ MeV. One can expect that the coherent photoproduction appears at $M_0 = M_{\Lambda^*} = 1.52$ GeV and that it is suppressed relative to the strong background when we go above or below this point. Since the cross section of the coherent photoproduction at $E_\gamma = 2$ GeV has bumps at $\theta_{\gamma\Lambda^*} \simeq 27.5^\circ$ and 152.5° in γd c.m.s. (see Fig. 9), then it is natural to expect that the regions around these angles are more favored for a manifestation of the coherence effect.

Note that at forward and backward angles of the pK^- pair photoproduction, $\theta_{\gamma(pK^-)}$, some of the spectator processes shown in Fig. 10 are suppressed dynamically. To illustrate this point, let us consider the dependence of $\cos\theta_{\gamma K^-}$ in $\gamma p \to \Lambda^* K^+$ photoproduction and $\cos\theta_{\gamma K^+}$ in $\gamma n \to \Theta^+ K^-$ photoproduction as a function of $\cos\theta_{\gamma\Lambda^*}$ (Fig. 16). Here we assume that $\theta_{\gamma K}$ is the K meson photoproduction angle in the γN c.m.s. and $\theta_{\gamma\Lambda^*}$ is the Λ^* photoproduction angle in γd c.m.s. One can see that the region of $0 \leqslant \theta_{\gamma\Lambda^*} \lesssim 76^\circ$ is forbidden kinematically for $\Theta^+ K^-$ photoproduction from the resting neutron. Similarly, the region of $107^\circ \lesssim \theta_{\gamma\Lambda^*} \leqslant \pi$ is forbidden for $\Lambda^* K^+$ photoproduction from the resting proton. In the kinematically forbidden regions the corresponding processes can proceed only through the high-momentum component in the deuteron wave function and, therefore, are exponentially small.

Consider first $\gamma d \to npK^+K^-$ photoproduction at a forward angle of the pK^- pair at $\theta_{\gamma(pK^-)} \simeq 27.5^\circ$ and $E_\gamma =$ 2 GeV. The corresponding invariant mass distributions for $M_0 = 1.52$, 1.57 and 1.47 are shown in Figs. 17(a)–17(c), respectively.

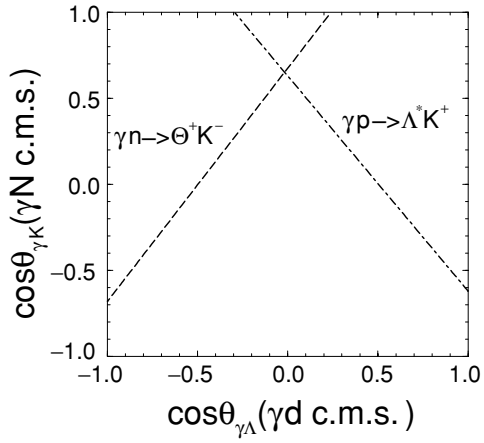

FIG. 16. Dependence of $\cos\theta_{\gamma K^-}$ in $\gamma p \to \Lambda^* K^+$ photoproduction and $\cos\theta_{\gamma K^+}$ in $\gamma n \to \Theta^+ K^-$ photoproduction as functions of $\cos\theta_{\gamma\Lambda^*}$ in the $\gamma d \to \Lambda^*\Theta^+$ reaction at $E_\gamma = 2$ GeV.

At $M_0 = M_{\Lambda^*}$, the background is dominated by the resonant Λ^* photoproduction in the spectator mechanism shown in Fig. 10(a). The next important contribution comes from the nonresonance spectator channel [Fig. 10(b)]. The shape of the background spectrum has a resonancelike behavior with the center close to the mass of Θ^+ and a width of about 15 MeV. This behavior is defined by the spectral distribution function W_{nK} (or the deuteron momentum distribution) in Eq. (27) and the kinematics [see Fig. 14(a)]. At $M_{pK^-} = 1.52$ GeV, W_{nK} has a sharp peak at $M_{nK^+} \simeq 1.54$ GeV. For $M_{pK^-} = 1.57$ and 1.47 GeV the peak position is shifted to lower or higher masses, respectively. Similarly, one can see the corresponding shift in the background contribution at $M_0 = 1.57$ and 1.47 GeV, shown in Figs. 17(b) and 17(c). Here, the background is dominated by the nonresonance spectator

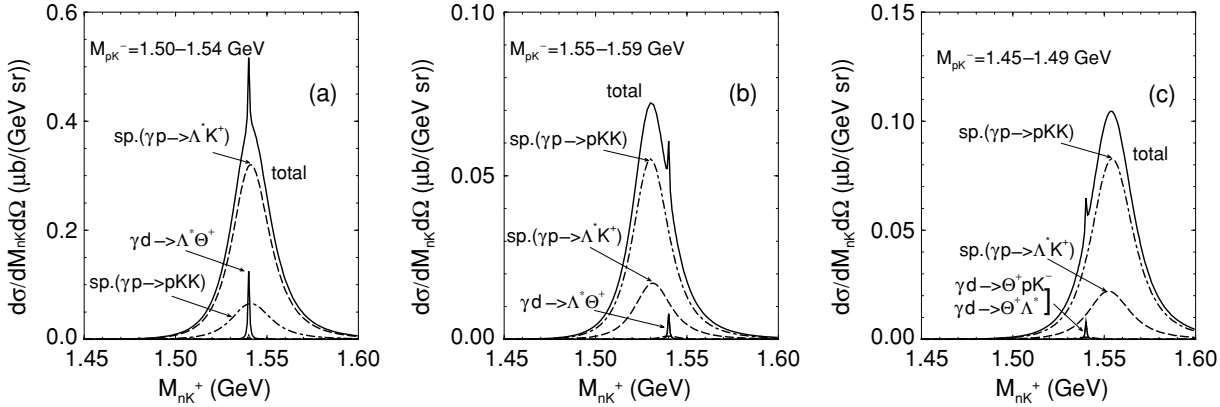

FIG. 17. The nK^+ invariant mass distribution in the $\gamma d \to npK^+K^-$ reaction at fixed values of the pK^- invariant mass. The angle of the pK^- pair photoproduction in γd c.m.s., $\theta_{\gamma(pK^-)} = 27.5^\circ$ and $E_\gamma = 2$ GeV. (a) $M_{pK^-} = 1.52 \pm 0.02$ GeV; (b) $M_{pK^-} = 1.57 \pm 0.02$ GeV, (c) $M_{pK^-} = 1.47 \pm 0.02$ GeV. The notation sp.($\gamma p \to \Lambda^* K^+$) and sp.($\gamma p \to pKK$) corresponds to the processes depicted in Figs. 10(a) and 10(b), respectively; $\gamma d \to \Theta^+ pK^-$ corresponds to the coherent background shown in Fig. 10(e), $\gamma d \to \Lambda^*\Theta^+$ corresponds to the coherent $\Lambda^*\Theta^+$ photoproduction (Fig. 7).

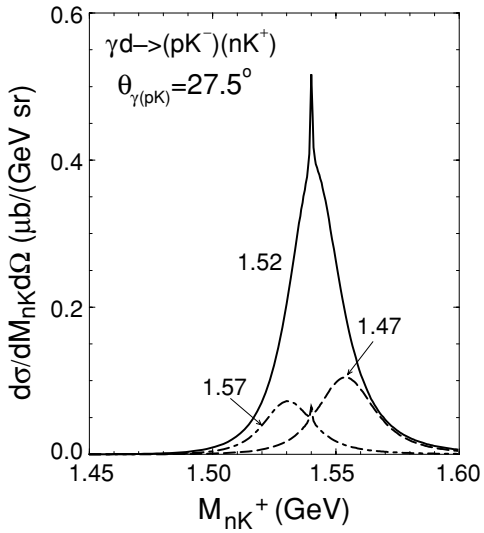

FIG. 18. Summary plot of the total nK^+ invariant mass distribution in the $\gamma d \to npK^+K^-$ reaction at three fixed intervals of the pK^- invariant mass with $M_0 = 1.52, 1.57$ and 1.47 (GeV) at $\theta_{\gamma(pK^-)} = 27.5^\circ$ and $E_\gamma = 2$ GeV.

channels. Its value is almost similar for all considered values of M_0, being much smaller than the total background at $M_0 = 1.52$ GeV.

At $M_0 = 1.52$ GeV, the height of the peak of the coherent $\Lambda^*\Theta^+$ channel is about one third of the total background contribution. This ratio decreases for $M_0 = M_{\Lambda^*} \pm 70$ MeV. Thus, a summary plot of the total nK^+ invariant mass distribution for three fixed intervals of the pK^- invariant mass is shown in Fig. 18.

One can conclude that, since the width of the coherent photoproduction is much smaller than the effective width of the background, this contribution can be extracted experimentally under the condition of a high-resolution measurement of the nK^+ invariant mass.

In the case of a energy resolution comparable with the width of the background peak, one has to smear this peak. The simplest way to do it is integrating the nK^+ invariant mass distribution over Ω in the forward hemisphere of the pK^- pair photoproduction. The corresponding predictions for $M_0 = 1.52$ GeV and a summary plot for three values of M_0 are shown in Figs. 19(a) and 19(b), respectively. One can see that again at $M_0 = M_{\Lambda^*}$ the background is dominated by the resonance Λ^* photoproduction where the neutron is a spectator. But the shape of the background is quite different from the previous case. Instead of the narrow peak one observes a monotonic increase of the background contribution. This behavior allows us to extract the sharp Θ^+ peak of the coherent $\Lambda^*\Theta^+$ photoproduction. The peak becomes negligible at $M_0 = M_{\Lambda^*} \pm 70$ MeV, as shown in Fig. 19(b). Here one can also see the prediction for a Gaussian smearing of the Θ^+ peak with $\sigma = 5$ MeV.

Consider now the backward hemisphere of the pK^- pair photoproduction in the reaction $\gamma d \to npK^+K^-$, say for $\theta_{\gamma(pK^-)} \simeq 152.5^\circ$. The corresponding invariant mass distributions at different M_0 are exhibited in Fig. 20.

Now, the dominant contribution to the background comes from the spectator resonant Θ^+ photoproduction, depicted in Fig. 10(c). The other channels are rather weak. At $M_0 = 1.52$ GeV the background contribution is enhanced by the distribution function W_{pK}, which at $M_{nK^+} \simeq 1.54$ GeV is much greater for $M_0 \simeq M_{\Lambda^*}$ [see Fig. 14(b)]. The coherent contribution of the $\Lambda^*\Theta^+$ photoproduction is a factor of four smaller than the background contribution.

The summary plot of the total invariant mass distribution of the nK^+ for three fixed intervals of the pK^- invariant mass is displayed in Fig. 21. One can see a strong increase of the invariant mass distribution at $M_0 = 1.52$ GeV. But this increase is caused mainly by the properties of the distribution function W_{pK}. Here, we have no striking qualitative effect of the coherent $\Lambda^*\Theta^+$ photoproduction. Therefore, studying the coherent $\Lambda\Theta^+$ photoproduction seems to be difficult in this kinematic region.

Now we make three comments. First, since in the forward hemisphere of the Λ^* photoproduction the dominant contribution comes from the backward angles of the K^+ photoproduction in the elementary $\gamma p \to \Lambda^* \bar{K}^+$ subprocess, our predictions are not sensitive to the choice of the solution for the coupling strength α_{Λ^*} discussed in Sec. II [see Fig. 6(b)].

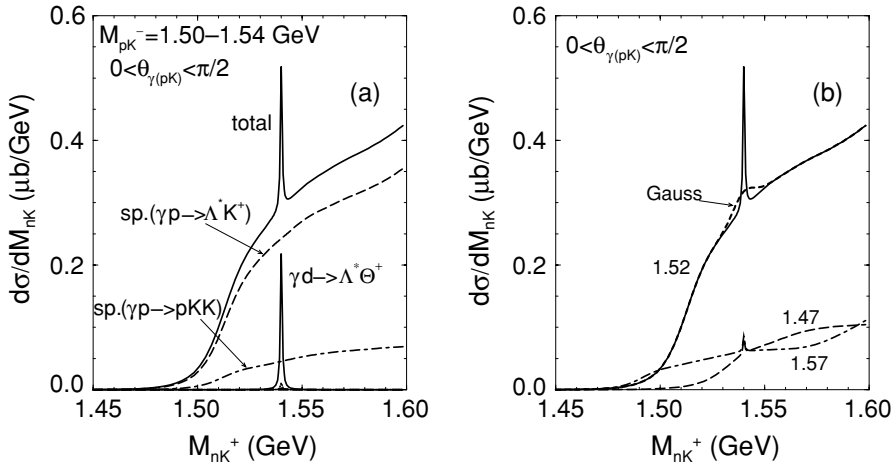

FIG. 19. (a) The nK^+ invariant mass distribution in the $\gamma d \to npK^+K^-$ reaction at $M_0 = 1.52$ GeV at the forward hemisphere of pK^- pair photoproduction and $E_\gamma = 2$ GeV. Notation is the same as in Fig. 17. (b) Summary plot of the total nK^+ invariant mass distribution at three fixed intervals of the pK^- invariant mass with $M_0 = 1.52, 1.57$ and 1.47 GeV.

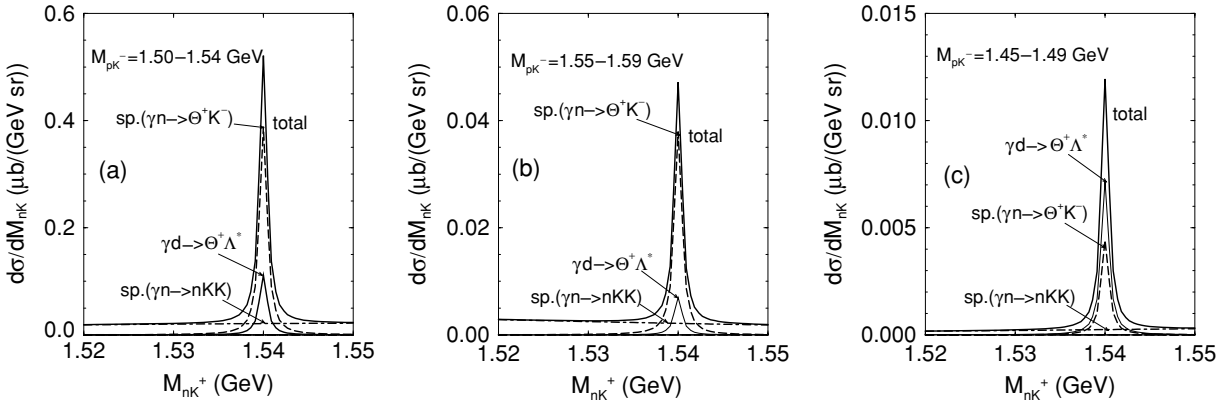

FIG. 20. Same as in Fig. 17 but for $\theta_{\gamma(pK^-)} = 152.5^\circ$. The notations sp.($\gamma n \to \Theta^+ K^+$) and sp.($\gamma n \to nKK$) corresponds to the processes depicted in Figs. 10(c) and 10(d), respectively.

Second, in our analysis we have assumed that the Θ^+ photoproduction from the nucleon is dominated by the t-channel K^* exchange process. This assumption leads to a similarity of the Θ^+ photoproduction from the neutron and proton. A violation of this similarity (or a suppression of the photoproduction from the proton, with the cross section of the $\gamma n \to \Theta^+ K^-$ kept on the same level) discussed recently [9,23] would result in a suppression of the process shown in Fig. 7(d). As a consequence, the coherent cross section of $\Lambda^*\Theta^+$ photoproduction would be suppressed around the second peak at the backward angles of the pK^- pair photoproduction, shown in Figs. 9 and 15, leaving the first peak at the forward-angle photoproduction without change. The corresponding calculation of the differential cross section with and without the contribution of the $\gamma p \to \Theta^+ \bar{K}^0$ subprocess is presented in Fig. 22. Since the coherent $\Lambda^*\Theta^+$ photoproduction is determined by the first peak, our main result shown in Fig. 19 remains unchanged.

Third, the bumplike structure of the differential cross section of the coherent $\gamma d \to \Lambda^*\Theta^+$ reaction is caused mainly by the spectral functions S in Eqs. (17). Thus in Eq. (17a) the amplitude of the $\Theta^+ \to nK^+$ transition is a smooth function compared with the spectral function S^{Λ^*} independently of the properties of Θ^+. Therefore, our predictions remain valid for the $J^P = \frac{3}{2}^{\pm}$ of Θ^+, considered in the recent Ref. [9].

When our prediction is to be compared with experiments, one should pay attention to at least the following two points. First, an energy spread in the beam photon may change the shape of the background, which is determined mainly by the quasi-free Λ^* production. However, our conclusion, as indicated by Fig. 19, is not changed qualitatively. Second, the shape of the background is sensitive to the acceptance of the measurement. In particular, the effect of coherent $\Lambda^*\Theta^+$ production may be significantly suppressed when the detector does not have the acceptance to detect the pK^- pair in the forward angles. In contrast, the acceptance of the forward

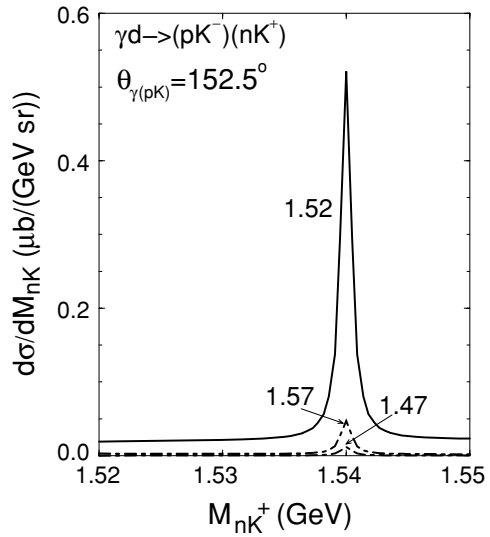

FIG. 21. Same as in Fig. 18 but for $\theta_{\gamma(pK^-)} = 152.5^\circ$.

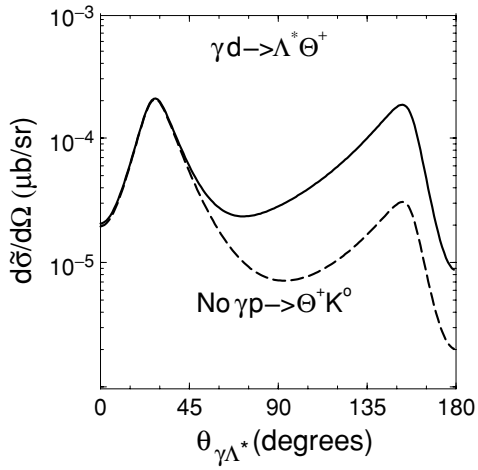

FIG. 22. Differential cross section of $\Lambda^*\Theta^+$ photoproduction with (solid curve) and without (dashed curve) the contribution of the $\gamma p \to \Theta^+ \bar{K}^0$ subprocess.

pK^-, as in the case of LEPS of SPring-8 [1], may make the effect more pronounced.

VI. SUMMARY

In summary, we analyzed the coherent $\Lambda^*\Theta^+$ photoproduction in γd interaction, taking into account different background processes. We found that the behavior and the strength of the background processes depend strongly on the kinematics, where the momentum distribution in the deuteron plays a key role. Thus, at fixed angle of the pK^- photoproduction the nK^+ invariant mass distribution of the background processes looks like a narrow peak with maximum around the Θ^+ mass. This behavior hampers the extraction of the coherent process at finite invariant mass resolution. Most promising is an experimental analysis of the distributions integrated over the pK^- production angles in the forward hemisphere of the c.m.s. In this case the background processes increase monotonically with M_{nK^+} in the vicinity of M_{Θ^+}, which allows us to extract the coherent $\gamma d \to \Lambda^*\Theta^+$ channel even with finite invariant mass resolution. We have demonstrated that the coherent $\Theta^+\Lambda(1520)$ photoproduction does not depend on the Θ^+ photoproduction amplitude but rather is defined by the probabilities of the $\Lambda(1520)$ photoproduction and the $\Theta^+ \to NK$ transition. Therefore, this effect may be used as an independent method for studying the mechanism of Θ^+ production and Θ^+ properties.

Our model estimates for the γd reaction may be considered an example of why the Θ^+ peak is seen under certain experimental conditions and why it does not appear above the strong background in others.

Finally, we note that the predicted process of the coherent $\Lambda^*\Theta^+$ photoproduction may be studied experimentally at the electron and photon facilities at LEPS of SPring-8, JLab, Crystal Barrel of the Electron Stretcher and Accelerator (ELSA) and GRAAL of the European Synchrotron Radiation Facility (ESFR).

We appreciate fruitful discussions with T. Nakano who initiated this study, and we thank H. Ejiri, M. Fujiwara, K. Hicks, and A. Hosaka for useful comments and suggestions. A. I. Titov thanks E. Grosse for offering the hospitality at Forschungszentrum Rossendorf e.V. (FZR). This work was supported by Bundesministerium für Bildung und Forschung (BMBF) grant 06DR121, GSI-FE.

APPENDIX: TRANSITION OPERATORS FOR THE RESONANCE AMPLITUDES

1. Θ^+ photoproduction amplitude

We show here the explicit expressions for the transition operators $\mathcal{M}_\mu$ in Eq. (5) for a positive Θ^+ parity and the PS coupling scheme.

The specific parameters for the form factor in Eq. (4) are defined by

$$F_s = F(M_N, s), \quad F_u = F(M_\Theta, u), \quad F_t = F(M_{K^+}, t). \quad \text{(A1)}$$

In addition, we need the form-factor combinations

$$\widetilde{F}_{tu} = F_t + F_u - F_t F_u, \quad \widetilde{F}_{su} = F_s + F_u - F_s F_u \quad \text{(A2)}$$

to construct the contact terms $\mathcal{M}^c_\mu$ given below that make the initial photoproduction amplitude gauge invariant [25,26]. The four-momenta in the following equations are defined according to the arguments given in the reaction equation

$$\gamma(k) + N(p) \to \Theta^+(p_\Theta) + \bar{K}(\bar{q}). \quad \text{(A3)}$$

a. $\gamma n \to \Theta^+ K^-$

$$\mathcal{M}^t_\mu = i\frac{e g_{\Theta NK}(k_\mu - 2\bar{q}_\mu)\gamma_5}{t - M^2_{K^+}} F_t, \quad \text{(A4a)}$$

$$\mathcal{M}^s_\mu = i e g_{\Theta NK}\gamma_5 \frac{\not{p} + \not{k} + M_N}{s - M^2_N}\left(i\frac{\kappa_p}{2M_N}\sigma_{\mu\nu}k^\nu\right)F_s, \quad \text{(A4b)}$$

$$\mathcal{M}^u_\mu = i e g_{\Theta NK}\left(\gamma_\mu + i\frac{\kappa_\Theta}{2M_\Theta}\sigma_{\mu\nu}k^\nu\right) \times \frac{\not{p}_\Theta - \not{k} + M_\Theta}{u - M^2_\Theta}\gamma_5 F_u, \quad \text{(A4c)}$$

$$\mathcal{M}^c_\mu = i e g_{\Theta NK}\gamma_5\left[\frac{(k - 2\bar{q})_\mu}{t - M^2_{K^+}}(\widetilde{F}_{tu} - F_t) + \frac{(2p_\Theta - k)_\mu}{u - M^2_\Theta}(\widetilde{F}_{tu} - F_u)\right]. \quad \text{(A4d)}$$

The transition operator of t-channel K^* exchange amplitude is given by

$$\mathcal{M}^t_\mu(K^*) = \frac{e g_{\gamma KK^*} g_{\Theta NK^*}}{M_{K^*}} \frac{\varepsilon_{\mu\nu\alpha\beta}k^\alpha \bar{q}^\beta}{t - M^2_{K^*}} \times \left[\gamma^\nu - i\frac{\sigma^{\nu\lambda}(p - p_\Theta)_\lambda}{M_\Theta + M_N}\kappa^*\right]F(M_{K^*}, t). \quad \text{(A5)}$$

b. $\gamma p \to \Theta^+ \bar{K}^0$

$$\mathcal{M}^s_\mu = i\frac{e g_{\Theta NK}}{M_\Theta + M_N}\gamma_5 \not{\bar{q}}\frac{\not{p} + \not{k} + M_N}{s - M^2_N} \times \left(\gamma_\mu + i\frac{\kappa_p}{2M_N}\sigma_{\mu\nu}k^\nu\right)F_s, \quad \text{(A6a)}$$

$$\mathcal{M}^u_\mu = i\frac{e g_{\Theta NK}}{M_\Theta + M_N}\left(\gamma_\mu + i\frac{\kappa_\Theta}{2M_\Theta}\sigma_{\mu\nu}k^\nu\right) \times \frac{\not{p}_\Theta - \not{k} + M_\Theta}{u - M^2_\Theta}\gamma_5 \not{\bar{q}} F_u, \quad \text{(A6b)}$$

$$\mathcal{M}^c_\mu = i\frac{e g_{\Theta NK}}{M_\Theta + M_N}\gamma_5 \not{\bar{q}}\left[\frac{(2p + k)_\mu}{s - M_N}(\widetilde{F}_{su} - F_s) + \frac{(2p_\Theta - k)_\mu}{u - M^2_\Theta}(\widetilde{F}_{su} - F_u)\right]. \quad \text{(A6c)}$$

2. Λ^* photoproduction amplitude

We show here the explicit expressions for the transition operators $\mathcal{M}_{\sigma\mu}$ in Eq. (8) for the reactions $\gamma p \to \Lambda^* K^+$ and $\gamma n \to \Lambda^* K^0$.

a. $\gamma p \to \Lambda^* K^+$

$$\mathcal{M}^t_{\sigma\mu} = i\frac{eg_{\Lambda^* NK} M^*_\Lambda (2q_\mu - k_\mu)(k_\sigma - q_\sigma)\gamma_5}{t - M^2_{K^+}} F_t, \tag{A7a}$$

$$\mathcal{M}^s_{\sigma\mu} = -i\frac{eg_{\Lambda^* NK}}{M^*_\Lambda} q^\sigma \gamma_5 \frac{\not{p} + \not{k} + M_N}{s - M^2_N} \times \left(\gamma_\mu + i\frac{\kappa_p}{2M_N}\sigma_{\mu\nu}k^\nu\right) F_s, \tag{A7b}$$

$$\mathcal{M}^c_{\sigma\mu} = i\frac{eg_{\Lambda^* NK}}{M^*_\Lambda}\gamma_5 \left[\frac{(2q-k)_\mu (k-q)_\sigma}{t - M^2_{K^+}} (\widetilde{F}_{ts} - F_t) - \frac{(2p+k)_\mu}{s - M_N}(\widetilde{F}_{ts} - F_s) + g_{\sigma\mu}\widetilde{F}_{ts}\right]. \tag{A7c}$$

The corresponding form factors are defined by

$$F_s = F(M_N, s), \quad F_t = F(M_{K^+}, t), \quad \widetilde{F}_{ts} = F_t + F_s - F_t F_s. \tag{A8}$$

The transition operator of t-channel K^* meson exchange amplitude is given by

$$\mathcal{M}^t_{\sigma\mu}(K^*) = \frac{eg_{\gamma KK^*} g_{\Lambda^* NK^*}}{M_{K^*} M_{\Lambda^*}} \frac{\varepsilon_{\nu\mu\alpha\beta}\, k^\nu q^\alpha}{t - M^2_{K^*}} \times [q'_\sigma \gamma_\sigma - \not{q}' g_{\sigma\beta}]\, F(M_{K^*}, t) \tag{A9}$$

with $q' = p_{\Lambda^*} - p$.

b. $\gamma n \to \Lambda^* K^0$

$$\mathcal{M}^s_{\sigma\mu} = -i\frac{eg_{\Theta NK}}{M^*_\Lambda} q^\sigma \gamma_5 \frac{\not{p} + \not{k} + M_N}{s - M^2_N}\left(i\frac{\kappa_p}{2M_N}\sigma_{\mu\nu}k^\nu\right) F_s. \tag{A10}$$

The t-channel K^*-exchange operator is defined by Eq. (A9) with the appropriate coupling constant $g_{\gamma KK^*}$.

[1] T. Nakano *et al.* (LEPS Collaboration), Phys. Rev. Lett. **91**, 012002 (2003).

[2] V. V. Barmin *et al.* (DIANA Collaboration), Phys. Atom. Nucl. **66**, 1715 (2003); Yad. Fiz. **66** 1763 (2003); S. Stepanyan *et al.* (CLAS Collaboration), Phys. Rev. Lett. **91**, 252001 (2003); V. Kubarovsky, *et al.* (CLAS Collaboration), *ibid.* **92**, 032001 (2004); J. Barth *et al.* (SAPHIR Collaboration), Phys. Lett. **B572**, 127 (2003); A. E. Asratyan, A. G. Dolgolenko, and M. A. Kubantsev, Phys. Atom. Nucl. **67**, 682 (2004). Yad. Fiz. **67**, 704 (2004).

[3] K. H. Hicks, arXiv:hep-ex/0504027, Prog. Part. Nucl. Phys. **55**, 647 (2005).

[4] S. Kabana, J. Phys. G **31**, S1155 (2005).

[5] T. Nakano, page 23 in *Proceedings of the International Workshop PENTAQUARK04, SPring-8*, edited by A. Hosaka and T. Hotta (World Scientific, Singapore, 2005); http://www.rcnp.osaka-u.ac.jp/penta04/.

[6] V. D. Burkert *et al.* (CLAS Collaboration), arXiv:nucl-ex/0408019.

[7] S.-I. Nam, A. Hosaka, and H.-C. Kim, arXiv:hep-ph/0503149; Phys. Rev. D **71**, 114012 (2005).

[8] A. I. Titov, H. Ejiri, H. Haberzettl, and K. Nakayama, Phys. Rev. C **71**, 035203 (2005).

[9] S.-I. Nam, A. Hosaka, and H.-C. Kim, arXiv:hep-ph/0505134.

[10] R. A. Arndt, I. I. Strakovsky, and R. L. Workman, Phys. Rev. C **68**, 042201(R) (2003); Erratum-*ibid.* **69**, 019901(E) (2004); J. Haidenbauer and G. Krein, *ibid.* **68**, 052201(R) (2003); A. Sibirtsev, J. Haidenbauer, S. Krewald, and U.-G. Meissner, Phys. Lett. **B599**, 230 (2004); A. Sibirtsev, J. Haidenbauer, S. Krewald, and U.-G. Meissner, Eur. Phys. J. A **23**, 491 (2005); A. Casher and S. Nussinov, Phys. Lett. **B578**, 124 (2004).

[11] S. Eidelman *et al.* (Particle Data Group Collaboration), Phys. Lett. **B592**, 1 (2004).

[12] K. Nakayama and K. Tsushima, Phys. Lett. **B583**, 269 (2004).

[13] Q. Zhao, Phys. Rev. D **69**, 053009 (2004); Erratum-*ibid.* D **70**, 039901 (2004).

[14] Q. Zhao and J. S. Al-Khalili, Phys. Lett. **B585**, 91 (2004); Erratum-*ibid.* **B596**, 317 (2004).

[15] S. I. Nam, A. Hosaka, and H. C. Kim, Phys. Lett. **B579**, 43 (2004).

[16] Y. Oh, H. Kim, and S. H. Lee, Phys. Rev. D **69**, 014009 (2004).

[17] W. Liu and C. M. Ko, Phys. Rev. C **68**, 045203 (2003); W. Liu and C. M. Ko, Nucl. Phys. **A741**, 215 (2004); W. Liu, C. M. Ko, and V. Kubarovsky, Phys. Rev. C **69**, 025202 (2004).

[18] Y. Oh, H. C. Kim, and S. H. Lee, Nucl. Phys. **A745**, 129 (2004).

[19] F. E. Close and Qiang Zhao, Phys. Lett. **B590**, 176 (2004).

[20] W. Roberts, Phys. Rev. C **70**, 065201 (2004).

[21] T. Mart, Phys. Rev. C **71**, 022202(R) (2005).

[22] Y. Oh, K. Nakayama, and T. -S. H. Lee, arXiv:hep-ph/0412363.

[23] R. De Vita *et al.* (CLAS Collaboration), talk presented at APS meeting, Tampa, April (2005).

[24] V. Guzey, Phys. Rev. C **69**, 065203 (2004).

[25] H. Haberzettl, Phys. Rev. C **56**, 2041 (1997); H. Haberzettl, C. Bennhold, T. Mart, and T. Feuster, Phys. Rev. C **58**, R40 (1998).

[26] R. M. Davidson and R. Workman, Phys. Rev. C **63**, 025210 (2001).

[27] Y.-R. Liu, P.-Z. Huang, W.-Z. Deng, X.-L. Chen, and Shi-Lin Zhu, Phys. Rev. C **69**, 035205 (2004).

[28] C. E. Carlson, C. D. Carone, H. J. Kwee, and V. Nazaryan, Phys. Rev. D **70**, 037501 (2004); F. E. Close and J. J. Dudek, Phys. Lett. **B586**, 75 (2004).

[29] S. Janssen, J. Ryckebusch, D. Debruyne, and T. Van Cauteren, Phys. Rev. C **65**, 015201 (2002); **66**, 035202 (2002).

[30] A. I. Titov and T.-S. H. Lee, Phys. Rev. C **66**, 015204 (2002).

[31] M. Benmerrouche, N. C. Mukhopadhyay, and J. F. Zhang, Phys. Rev. D **51**, 3237 (1995).
[32] D. P. Barber *et al*., Z. Phys. C **7**, 17 (1980).
[33] P. D. B. Collins, *An Introduction to Regge Theory and High Energy Physics* (Cambridge University Press, Cambridge, U.K., 1977).
[34] M. Lacombe, B. Loiseau, R. Vinh Mau, J. Cote, P. Pires, and R. de Tourreil, Phys. Lett. **B101**, 139 (1981); M. Lacombe, B. Loiseau, J. M. Richard, R. Vinh Mau, J. Cote, P. Pires, and R. de Tourreil, Phys. Rev. C **21**, 861 (1980).
[35] Aachen-Berlin-Bonn-Hamburg-Heidelberg-München Collaboration, Phys. Rev. **188**, 2060 (1969).